Untangling Glioblastoma Invasion:
Characterizing a Cell Culture Model of Glioblastoma Tumor Microtubes

Danny Jomaa

Supervisor: Dr. Ian Lorimer

This thesis is submitted to the
Faculty of Graduate and Postdoctoral Studies
in partial fulfillment of the requirements for the
Master's degree in Biochemistry

Department of Biochemistry, Microbiology & Immunology
Faculty of Medicine
University of Ottawa

Abstract

Glioblastoma is the most common and most lethal primary brain tumor to affect adults. While current treatment options provide temporary recourse, the majority of patients experience tumor recurrence and few survive five years past their initial diagnosis. Recently, tumor microtubes (TMs) were identified in an *in vivo* model of glioblastoma. These membrane-bound structures formed physical connections between tumor cells, over short and long distances, and facilitated intratumoral communication, invasion, treatment resistance, and post-treatment tumor recovery. To date, this is the first instance of TMs being reported in glioblastoma. The lack of an *in vitro* model for these structures has delayed further characterization of how TMs form between cells, facilitate intercellular exchange, and how they can be therapeutically targeted to increase treatment susceptibility. The study presented here is the first instance of TMs characterized in an *in vitro* model of primary glioblastoma (PriGO) cells. These TMs recapitulated many of the structural and functional properties of those observed *in vivo*, making it a suitable model for further experimentation. Using this model, Rac1, a known orchestrator of cytoskeletal remodeling and motility, was shown to be integral to establishing a TM network between PriGO cells, as demonstrated by siRNA-mediated protein knockdowns. PREX1, a GEF necessary for Rac1 signaling activity, also played a role in PriGO TM formation as evidenced by CRISPR/Cas9-based knockouts. Re-introducing a *PREX1* domain with Rac-GEF activity into cells lacking the protein led to a functional rescue of TM growth, thus confirming PREX1's involvement. Characterizing a cell culture model of glioblastoma TMs is a necessary first step in the study of these structures, ultimately paving the way for future development of therapies that disrupt this network.

Acknowledgements

First, I would like to thank my supervisor, Dr. Ian Lorimer, for the opportunity to develop new and exciting projects in the lab. I am grateful for the support and mentorship that Ian provided throughout my Master's and over the course of numerous experimental hurdles. My experience in Ian's lab has guided my academic pursuits and pushed me to excel.

I would also like to thank Sylvie, our lab tech, for the encouraging and supportive presence that she brings to the lab. Sylvie taught me most of the technical lab skills that I know and her willingness to help meant that I always had someone to turn to when I needed a helping hand.

I want to also thank the friends – Marina, Emma, Robyn, Anthea, Elaine – that were an unending source of love, support, and kindness over the last two years. Talking to you when challenges arose gave me the space to slow down and the resilience to take things one step at a time. Finally, Adam, you have been an unending source of motivation, support, and enthusiasm, and you've shared in the highs and lows of this journey. Thank you for being there for me through all of it.

Table of Contents

List of Abbreviations

ADP	Actin-Driven Protrusion
CRISPR	Clustered Regularly Interspaced Short Palindromic Repeats
crRNA	CRISPR RNA
Cx43	Connexin 43
DEP	Disheveled, EGL-10, and Pleckstrin Homology
DH	Dbl Homology
GAP	GTPase Activating Protein
G-CIMP	Glioma-CpG Island Methylator Phenotype
GEF	Guanine Exchange Factor
GFP	Green Fluorescent Protein
gRNA	Guide RNA
GSC	Glioma Stem Cell
GTIC	Glioma Tumor-Initiating Cell
KO	Knockout
NHEJ	Non-homologous End Joining
nMMIIA	Non-Muscle Myosin IIA
PAM	Protospacer Adjacent Motif
PH	Pleckstrin Homology
PIP_2	Phosphatidylinositol-4,5-biphosphate
PIP_3	Phosphatidylinositol-3,4,5-trisphosphate
PREX1	PIP_3-dependent Rac Exchange Factor 1
PriGO	Primary Glioblastoma Cells

Rac1	Ras-related C3 botulinum toxin substrate
T7EI	T7 Endonuclease I
TCGA	The Cancer Genome Atlas
TIDE	Tracking of Indels by DEcomposition
TM	Tumor Microtube
TMZ	Temozolomide
TNT	Tunneling Nanotube
tracrRNA	trans-activating CRISPR RNA

List of Figures

1. Introduction

4. Results

5. Discussion

6. Appendix

1. Introduction

1.1. Glioblastoma

1.1.1. Classification

Primary malignant gliomas are a family of tumors named for their *de novo* growth in the brain and their histologic and morphologic similarity to normal glial cells (1). The World Health Organization classifies tumors of the central nervous system on a 4-grade histological scale defined by increasing degrees of undifferentiation, aggressiveness, and mortality (1,2). On this scale, glioblastoma is a grade IV glioma and accounts for approximately 80% of glioma cases. Glioblastoma is also the most common primary brain tumor to affect adults; each year, approximately 1,000 Canadians are diagnosed with glioblastoma, most commonly at the age of 60 or older (2,3). Clinical signs of glioblastoma include headaches, cognitive difficulties, personality changes, gait imbalance, focal signs, and seizures (4). Histologically, glioblastoma presents with dense cellularity, a high mitotic index, extensive vascularity, and tissue necrosis (1). Despite extensive interventions, 90% of patients experience tumor recurrence within seven months, and fewer than 5% of patients survive five years after their diagnosis (5).

A defining feature of this disease is its ability to grow rapidly, infiltrate tissue, and disseminate across the brain (6). Histological analysis has shown that this predominantly occurs along existing brain structures, named Scherer's secondary structures. These include cerebral blood vessels, white matter tracts, and the subarachnoid space (5). Bradykinin produced by cerebrovascular endothelial cells is known to act as a chemotactic signaling peptide to glioblastoma cells, directing their movement towards blood vessels. In mouse models of glioma, icatibant, a bradykinin receptor inhibitor, has been shown to reduce the percentage of vessel-adhered glioma cells by 58%, suggesting that targeting the glioblastoma microenvironment could be one therapeutic option (7). Expansion of the tumor can begin with as little as one cell migrating

outwards from the tumor bulk; this diffuse invasion of the surrounding brain tissue is often responsible for incomplete surgical resection and subsequent recurrence of the tumor, typically within a few centimeters of the original tumor border (8).

1.1.2. Diagnosis and treatment

The current standard of care for glioblastoma is a combination of maximal surgical resection, radiotherapy, and the chemotherapeutic agent temozolomide (TMZ) (9). TMZ, the major first-line therapy for patients with this disease, was first used to treat primary brain tumors in 1993 (10). TMZ's cytotoxicity comes from its ability to methylate DNA at the N^7 and O^6 positions of guanine, as well as the N^3 position of adenine (11). Activation of the DNA repair response occurs but, unable to find a corresponding base, leaves nicks in the DNA strand (12). These nicks accumulate and block the cell cycle at the G_2-M DNA damage checkpoint, ultimately triggering apoptosis when cells cannot complete mitosis (13). The enzyme O^6-methylguanine-DNA methyltransferase (MGMT) plays a primary role in TMZ resistance by demethylating O^6-methylguanine sites, effectively reversing the cytotoxic activity of TMZ lesions (14). In line with this, epigenetic silencing of the *MGMT* gene, observed in approximately 45% of glioblastoma cases, has been correlated with responsiveness to therapy (14,15). Indeed, in patients with silenced *MGMT*, a significantly longer median survival is observed after treatment with TMZ and radiotherapy compared to patients receiving only radiotherapy (21.7 months vs. 15.3 months, respectively) (14).

Since the introduction of TMZ, a number of adjuvant therapies have been developed and reserved for salvage treatment after tumor recurrence. Among these are bevacizumab, a vascular endothelial growth factor (VEGF)-targeting antibody that inhibits tumor angiogenesis; irinotecan, a chemotherapeutic agent that has been combined with bevacizumab to extend progression-free survival; and procarbazine, lomustine, vincristine (PCV), a ternary drug cocktail with a high

toxicity profile and similar mechanism of action to TMZ (1,16–18). Despite the availability of these therapies, they have done little to extend overall survival for patients with glioblastoma, often work in a small subset of patients, and come with a host of toxicities and side-effects that reduce patients' quality of life both during and after treatment (16). Indeed, the challenge in developing more targeted therapeutic approaches has been credited to several factors: 1) intratumoral genetic heterogeneity; 2) tumor dissemination into intricate brain regions, making complete surgical resection unachievable in most cases; 3) physiological isolation of the tumor due to the blood-brain barrier; and 4) challenges identifying and targeting self-renewing glioblastoma stem cells (GSCs) (19,20). Thus, while it is true that clinicians' therapeutic repertoire has expanded, the lack of robust and durable treatment options emphasizes the need for a more thorough comprehension of the disease's molecular drivers.

1.1.3. Genetics of glioblastoma

Cases of glioblastoma can be divided into clinical and molecular subtypes. Clinical subdivision distinguishes between primary tumors that typically develop *de novo* in older patients with no history of astrocytoma, and secondary tumors that originate from low-grade astrocytoma tumors and are often seen in younger patients (2,21). Primary and secondary glioblastoma tumors differ broadly in their genetic make-up. Primary tumors frequently harbor *TERT* mutations, *EGFR* amplification, and loss of *PTEN, INK4A* and *NF1*. In contrast, secondary tumors are marked by *TP53* and *IDH1/2* mutations, *PDGF* and *FGF* amplification, and *PTEN* and *RB* loss (21,22).

In 2008, The Cancer Genome Atlas (TCGA) performed an extensive genetic and epigenetic analysis of over 200 tumors and constructed a molecular classification scheme that divided glioblastoma into four subtypes based on expression profile clustering (23). Analysis of the mutations associated with each subtype revealed the following: classical tumors were

characterized by *EGFR* amplification, lack of *TP53* mutation, and *CDKN2A* deletion; neural tumors by elevated expression of neuronal markers *NEFL, GABRA1, ASCL1*, and *TCF4*; proneural tumors harbored amplification of the *PDGFRA* gene, mutations to *IDH1* and *TP53*, and increased expression of several proneural development genes, such as *SOX, DCX, DLL3,* and *TCF4*; and mesenchymal tumors exhibited *NF1* mutation, expression of tumor necrosis factor (TNF) and NF-κB pathway genes, and mesenchymal marker expression, including *MET* and *CHI3L1* (23,24). A fifth subtype has been identified since the first molecular classification–the glioma-CpG island methylator phenotype (G-CIMP)–which refers to tumors with hypermethylation of the *MGMT* promoter-associated CpG island (25,26). This subtype makes up a large portion of secondary tumors and accounts for their increased sensitivity to TMZ treatment (25). The phenotype is also dependent on the presence of mutations to the isocitrate dehydrogenase 1 (*IDH1*) gene (27–29).

The abundance of molecular subtypes clearly showcases glioblastoma's extensive genetic heterogeneity, however a number of mutations still prevail across classifications. Among these are mutations to *TP53*, a tumor suppressor protein which responds to DNA damage by activating cellular stress pathways that halt the cell cycle and induce apoptosis (30). The TP53 pathway is mutated in approximately 87% of patients, and most often in those with secondary tumors (31). This predominantly occurs through deletion of the *CDKN2A* locus (58%), followed by mutation or deletion of the *TP53* gene (28%) (32). Mutations to the epidermal growth factor receptor (EGFR) and platelet-derived growth factor receptor (PDGFR)–both members of the receptor tyrosine kinase (RTK) family of extracellular signaling receptors–are seen in approximately 45% and 13% of GBM patients, respectively (33). This class of receptors controls the MAPK and PI3K pathways which are critical mediators of cell survival, proliferation, differentiation, and angiogenesis (33). Downstream of RTKs, Phosphatase and tensin homologue located on

chromosome TEN (PTEN) downregulates cell cycle progression by reducing intracellular levels of phosphatidylinositol-3,4,5-trisphosphate (PIP_3), thus limiting cell growth and division (30). 80% of patients with glioblastoma have lost one allele of *PTEN* and the second allele is deleted or mutated in 40% of cases (34). Conversely, mutations to *PI3K*, the enzyme responsible for PIP_3 production, are observed in approximately 25% of glioblastoma patients and lead to constitutive signaling of the PI3K pathway (32). Similarly, mutations to the tumor suppressor retinoblastoma (RB) are seen in 20% of patients with glioblastoma (30). The RB protein is critically involved in inhibiting progression of the cell cycle by binding to, and inhibiting, members of the E2F family of transcription factors (30). Signaling mutations can also be used as predictors of survival and prognosis. For example, deletion of exons 2-7 in the *EGFR* gene (referred to as *EGFRvIII*) correlates strongly with poor prognosis for affected patients (35).

Delineating the genetic and clinical profile of different subtypes has been an important step forward for glioblastoma research. Identifying unique molecular subtypes that are associated with different treatment sensitivities and clinical outcomes has laid the groundwork for personalized approaches to treating glioblastoma in the future.

1.1.4. Primary glioblastoma cultures

The results presented here make use of primary glioblastoma cells that were isolated from patients undergoing surgical tumor resection at The Ottawa Hospital. Referred to here as PriGO cells, these cultures were grown in monolayers on laminin-coated plates using serum-free Neurobasal A (NA) media supplemented with epidermal growth factor (EGF), fibroblast growth factor 2 (FGF2), B-27 supplement, and N-2 supplement at 37˚C in 5% O_2. Incubation in 5% O_2 supports PriGO cell growth more than atmospheric oxygen levels (~20%), likely due to the similarity to physiological oxygen levels in the brain (36). In previous studies, glioblastoma cells

that were isolated from patients and grown in similar conditions have been referred to as glioma stem cells (GSCs) and glioblastoma tumor-initiating-cells (GTICs). These conditions preserve the genetic and molecular profile of PriGO cells *in vitro*, as well as their invasive phenotype when injected as intracranial xenografts into immunocompromised mice (36–38). Primary glioblastoma cultures have also been shown to express several neural stem cell markers *in vitro*, including SOX2, Nanog, Musashi-1, inhibitor of differentiation protein 1 (ID1), Olig2, and nestin, and are capable of differentiating into neurons, astrocytes, and oligodendrocytes (39–43). A number of cell surface proteins have been proposed as markers to enrich GSCs from non-stem tumor cells, including CD133, CD15, CD44, and A2B5 (44–46). However, these markers are reported to mediate interactions between glioblastoma cells and their microenvironment, thus dissociating these cells can alter the type and pattern of marker expression.

A number of studies have successfully identified lineage-specific signaling pathways that direct GSC differentiation. For example, treating GSCs with Wnt3a, an inhibitor of Notch signaling, has been shown to induce βIII-tubulin^{+} neuronal differentiation (47). This could also be accomplished by overexpression of the transcription factor *ASCL1*, which in turn increases expression of genes such as *MYT1, GPR37L1,* and *HMGA2* (48). Treating GSCs with bone morphogenic protein 4 (BMP4) has also been shown to direct GFAP^{+} astrocytic lineage differentiation and reduce tumorigenicity (49). However, many of these cells remain susceptible to cell cycle re-entry and do not exhibit the appropriate reconfiguration of DNA methylation patterns (50). Serum-induced differentiation has been associated with the expression or co-expression of several distinct lineage markers, including GFAP (astrocytic) and TuJ1 (neuronal), in PriGO cells and other GSC lines (36,39,51). Indeed, culturing glioblastoma cells in serum-containing media also causes an eventual loss of invasive phenotype, both *in vitro* and *in vivo* (52).

1.2. Bridging cells with physical connections

1.2.1. Tunneling nanotubes

Dynamic cell-to-cell connections were first reported in rat pheochromocytoma PC12 cells (53). These structures were termed tunneling nanotubes (TNTs) for their ability to physically connect cells over long distances and form open-ended, 'tunnel-like' tubes that facilitate the intercellular exchange of organelles, vesicles, proteins, calcium, miRNA, ATP, and other cargo (54). They are further distinguished from other cellular extensions by forming above, and being non-adherent to, the culture plate surface (55,56). *In vitro*, TNTs are observed to have a diameter of 20-500nm and extend up to several hundred micrometers in length (57). Since their discovery, TNTs have been reported in numerous healthy and cancerous cell lines, including NRK cells, B cells, macrophages, cardiac myocytes, ovarian cancer cells, and mesothelioma cells (58–61). TNTs have also been seen connecting normal and cancer cells, including ovarian epithelial cells and ovarian cancer cells, osteoblast cells and osteosarcoma cells, and HeLa cells and fibroblasts (60,62). The degree of exchange permitted by TNTs has been shown to vary according to the membrane continuity between cells (63). Open-ended TNTs define those that permit uni- or bi-directional transfer of cellular cargo, while close-ended TNTs form a junctional boundary between cells that allows select cargo transfer. For example, TNTs connected by connexin 43-containing gap junctions are able to exchange calcium ions and other small molecules between cells (63,64).

While the function of TNTs has largely been shown to facilitate positive intercellular communication, these structures can also be used as a conduit for the transfer of non-beneficial cargo. TNTs have been observed to allow the transfer of prions (PrP^{Sc}) between infected and uninfected neuronal CAD cells, as well as between dendritic cells and primary neurons (65). This may represent a novel route for prions to access the nervous system. TNTs have also been reported

to transfer the fibrillar protein Tau between neurons, thus possibly contributing to Tau aggregate pathologies, such as Alzheimer's disease (66). More recently, TNTs were also implicated in the transfer of HIV between primary macrophages (64).

Several studies have evaluated the structural properties of TNTs and the signaling pathways necessary for their growth. TNTs ubiquitously contain F-actin, allowing dynamic cytoskeletal reorganization, but vary with regards to the presence of microtubules (67). In Raw264.7 macrophage cells, M-Sec was identified as a critical component of TNT formation via its interaction with RalA and the downstream exocyst complex that initiates cytoskeletal remodeling (68). Similar work in RAW/LR5 macrophage cells demonstrated that both Cdc42 and Rac1 play important roles in TNT biogenesis and elongation (55). Inhibiting the function of either protein significantly reduced the number of TNT-like protrusions observed, and depletion of their downstream effectors, Arp2/3 and WAVE, similarly impaired the number of TNT connections that formed between cells (55). Using 3D super-resolution imaging, the same study identified differential localization of Cdc42 and Rac1 within TNTs. Specifically, Cdc42 was concentrated at the structure base while Rac1 was observed throughout the TNT length, suggesting a differential role for both proteins in the formation and maintenance of TNTs. In contrast to these findings, studies performed in CAD cells demonstrate that Cdc42, IRSp53, and VASP all act to stimulate filopodia growth while simultaneously inhibiting the formation of TNTs (57). The same study found a reverse role for Eps8, an actin-remodeling protein, which facilitated TNT formation and reduced filopodia extension. Thus, this demonstrates that the mechanisms involved in TNT growth can differ depending on the cellular context and warrant cell type-specific characterization.

Previous reports have shown that cells are capable of forming TNTs by two mechanisms, both of which are supported by time-lapse video recordings (69). According to the cell

dislodgement mechanism, when two cell bodies come into physical contact, they move apart and retain a TNT between one another. In contrast, the actin-driven protrusion (ADP) mechanism describes instances where two separate cells extend filopodia-like protrusions that come into contact with one another and form a TNT bridge (63). Alternatively, TNTs can also form via the ADP mechanism when one cell extends a protrusion that comes into contact with the cell body of another cell. One study performed in rat hippocampus astrocytes identified S100A4, an extracellular signaling molecule, as a necessary cue for the growth of TNTs (70). The S100A4 receptor, Receptor for Advanced Glycation End Product (RAGE), was also required to successfully form TNTs (70). This suggests that the growth of cellular protrusions preceding TNTs is a non-random and coordinated process that depends on specific signaling cues and receptors.

1.2.2. Tumor microtubes

Studies of TNTs have mostly been conducted *in vitro*; however, structures with similar properties to TNTs were recently characterized in an *in vivo* model of glioblastoma (71). This study used patient-derived glioblastoma cells that were transplanted into mouse brains and followed by *in vivo* multiphoton laser-scanning microscopy (71). The authors referred to these physical connections as tumor microtubes (TMs) in light of their thicker diameter and ability to form ultra-long connections (>500μm), persist for long periods of time, and establish a multicellular functional network. TMs contained actin, β-tubulin, non-muscle myosin IIA, and mitochondria. Rather than a continuous membrane and cytoplasm, cells were separated by connexin 43 (Cx43)-containing gap junctions. These gap junctions were important for bidirectional propagation of intercellular calcium waves and required for long-term stabilization of TMs, as demonstrated by shRNA-mediated Cx43 knockdown. This further suggests that other

gap junction-permeable molecules, such as ATP and amino acids, may also participate in TM transfer, but this has yet to be explored.

Formation of TMs required activity of growth associated protein 43 (GAP-43)–a protein that is highly expressed in axonal growth cones and has a role in neuronal cell migration (71–73). Knockdown of GAP-43 significantly interfered with TM formation, resulting in shorter and less branched TMs, and smaller whole-tumor volume. The presence of TMs also correlated with cells' susceptibility to radiation-induced damage; TM-connected cells were protected from cell death compared to their non-connected counterparts via their ability to rapidly shuttle calcium ions to connected cells to prevent calcium-induced apoptosis. Furthermore, when cells were successfully ablated by laser-induced damaged, they were rapidly replaced by nuclei traveling to the damaged site via TMs (71). Indeed, the ability of TMs to be used as a conduit for nuclear migration in this study also implicates these structures in tumor dissemination and network expansion.

1.2.3. Other cellular extensions

TNTs and TMs are two of the numerous cellular extensions that have been characterized *in vitro* and *in vivo*. Included in this list are axons, astrocytic processes, cytonemes, filopodia, lamellipodia, invadopodia, and others. In many ways, TNTs and TMs are differentiated from these structures by morphological, functional, and signaling-related characteristics, however some degree of overlap has also been observed. In an effort to better elucidate the similarities and differences between these structures, as well as the qualities that uniquely set TNTs and TMs apart, a comparative table can be found below.

	Originally Reported In	Observed In	Identifying Structural Characteristics	Signaling Origins	Functions
Tunneling Nanotubes (TNTs)	Rat pheochromocytoma cells (PC12 cells) (53)	NRK cells, B cells, macrophages, cardiac myocytes, ovarian cancer cells, mesothelioma, osteosarcoma (58–61)	Actin-based, connect cells together, and form above the substrate (54)	Cell type-specific; Cdc42 and Rac1 +/-, Arp2/3, WAVE, VASP, Eps8 (54,55,57)	Facilitate intercellular transfer of organelles, vesicles, proteins, small molecules, ions, etc (63)
Tumor Microtubes (TMs)	Glioblastoma cells (71)	Glioblastoma cells (71)	Thicker and longer versions of TNTs that form in glioblastoma *in vivo* and persist for longer than TNTs (71,74)	GAP-43; presumably signaling also overlaps with TNT signaling pathways (71)	Facilitate bidirectional exchange of calcium ions between Cx 43-containing gap junctions (71)
Axons	Neurons	Neurons	Single axon per neurons; ranges from a single T-shape branch to elaborate arborization (75)	PARs for polarization; Spectrins and Ankyrin B at AIS; branching guided by neurotrophins (76)	Transmit electrical signals in the form of action potentials towards the synapse (77)
Astrocytic Processes	Astrocytes	Astrocytes	Star-shaped morphology, extend numerous processes to surround neurons, contain intermediate filaments (78)	Stellation is promoted by GPCR signaling, cAMPi, and MLCK activity, inhibited by RhoA (79)	Support neurons and neural transmission, e.g. K^+ buffering, clearance of glutamate, pH control, etc. (80)
Cytonemes	*Drosophila* wing imaginal disc (81)	*Drosophila* tissues (82)	Long cellular extensions that are defined by their orientation towards the disc midline where Dpp is expressed (82)	Require leucine-rich-GPCRs (Lgr4/5), VASP, fascin, and myosin-X (83)	Specialized filopodia that transport signaling proteins (e.g. morphogens) between signaling cells (82)
Filopodia	Metazoa (84)	Macrophages, neurons, epithelial cells (85)	Finger-like protrusions that form at the leading edge of cellular extensions (85)	Cdc42 stimulates Arp2/3 activity via WASP; RIF via Dia2; IRSp53 acts via WAVE2/ENA/VASP (85)	Migration, responding to chemoattractants, wound healing, cell-cell adhesion (86)
Lamellipodia	Metazoa (84)	Macrophages, neurons, epithelial cells (85)	Sheet-like protrusions typically found between filopodia (85)	Cdc42 stimulates Arp2/3 activity via WASP; cortactin scaffolding; cofilin, LIMK activity (85,87)	Migration, responding to chemoattractants, wound healing, cell-cell adhesion (86)

Abbreviations: PAR, partition-defective proteins; AIS, axon initial segment; MLCK, myosin light chain kinase; RIF, Rho in filopodia

Table 1. Comparison of TNTs and TMs to other cellular projections.

TNTs and TMs are presented with five other types of structures that are prominently featured in literature surrounding cellular extensions. An overview of the cells that have been reported to form each extension, as well as the extensions' identifying structural characteristics, signaling origins, and posited functions are presented as well. The comparison highlights a degree of overlap between TNTs, TMs, and other structures, but importantly, also sheds light on the unique characteristics that set TNTs and TMs apart.

1.3. The PI3K signaling pathway

1.3.1. Overview

The phosphatidylinositol-4,5-bisphosphate 3-kinase (PI3K) pathway is involved in cell survival, proliferation, and migration (88). This pathway begins with activation of an upstream receptor tyrosine kinase (RTK), such as the epidermal growth factor receptor (EGFR) or the platelet-derived growth factor receptor (PDGFR) (89). Upon ligand binding, the RTK catalyzes the activation of PI3K, allowing it to relocate to the cell membrane and phosphorylate phosphatidylinositol-4,5-bisphosphate (PIP_2) to form phosphatidylinositol-3,4,5-trisphosphate (PIP_3) (90). PIP_3-dependent Rac exchange factor 1 (PREX1) is synergistically activated by binding of PIP_3 and $G_{\beta\gamma}$, a product of G-protein-coupled receptor (GPCR) activation (90). Upon binding of both activators, PREX1 functions as a Rac guanine exchange factor (Rac-GEF), converting Rac1 from its inactive GDP-bound state to its active GTP-bound state (90). Once GTP-bound, Rac1 activates a number of downstream effector proteins that promote survival, proliferation, cytoskeletal reorganization, motility, and migration, as described below (91).

1.3.2. Rac1 and PREX1

The Ras superfamily is a collection of small GTPase proteins, subdivided into the Ras, Rho, Rab, Ran, and Arf subfamilies (92). Among the Rho family are RhoA, Cdc42, and Rac which have significant structural homology, bind some of the same interacting partners, and share related functions (93). Most notably, Rho family GTPases drive similar aspects of cytoskeletal reorganization. RhoA promotes the formation of stress fibers, Cdc42 initiates the formation of finger-like membranous protrusions, termed filopodia, and Rac drives formation of fan-like sheets that separate filopodia and propel cells forward during migration (94). The Rac subgroup of the Rho family consists of three isoforms: Rac1, Rac2, and Rac3. Only Rac1 is expressed ubiquitously,

while Rac2 and Rac3 expression is restricted to hematopoietic cells and neural cells, respectively (95). Like all GTPases, Rac1 cycles between GDP- and GTP-bound conformations. When bound to GTP, Rac1 is active and capable of interacting with effector proteins to orchestrate pro-survival and pro-migratory cellular functions (91). GTPase activating proteins (GAPs) accelerate the hydrolysis of GTP to GDP, thereby limiting the duration of Rac1 activity and converting Rac1 to its inactive state (96). These proteins include SRGAP3, RACGAP1, and ARHGAP15. In contrast, guanine exchange factors (GEFs), which include DOCK1, TIAM1, and PREX1, catalyze the exchange of GDP for GTP, thus promoting GTPase activity (96).

Phosphatidylinositol-3,4,5-trisphosphate (PIP_3)-dependent Rac exchange factor 1 (PREX1) is a member of the PREX family of Rac guanine exchange factor (Rac-GEF) proteins, which also encompasses PREX2 and its splice variant, PREX2b (90). The *PREX1* gene is located on chromosome 20 (20q13.13) and encodes 40 exons; its protein is 185kDa and is composed of 1,659 amino acids (90). The first domain in the PREX1 protein is a N-terminal Dbl homology (DH) domain which, in combination with the neighboring pleckstrin homology (PH) domain, enacts the protein's Rac-GEF catalytic activity. Following this are two Dishevelled, Egl-10, and Pleckstrin (DEP) domains and two PDZ protein interaction domains, as well as an inositol polyphosphate 4-phosphatase domain with no detectable phosphatase activity (90).

PREX1 was first discovered in neutrophils as a potent activator of Rac1 in the presence of PIP_3 (97). Since then, high levels of PREX1 expression have been detected in macrophages, platelets, and endothelial cells. Expression of PREX1 has been detected ubiquitously in the brain, and to a lesser degree in bone marrow, thymus, spleen, lymph node, and lung tissue (90). PREX1 was subsequently shown to be activated synergistically by both PIP_3 and $G_{\beta\gamma}$; activation by either component alone resulted in a one- to two-fold increase in PREX1-induced Rac1 activity, whereas

the presence of both activators increased Rac1 activity 16-fold (97). This is dependent on the DH and PH domains of Rac1, which bind $G_{\beta\gamma}$ and PIP_3, respectively (90).

The effect of *PREX1* deletion has been investigated in *PREX1*-knockout (*PREX1*-KO) mice (98). Mice lived normal life spans and were fertile but weighed approximately 14% less than wild-type mice. The most evident effect of *PREX1*-KO was observed in neutrophil responses. Neutrophils exhibited reduced GPCR-dependent, but not GPCR-independent, reactive oxygen species (ROS) production. After treating mice with an inflammatory agent, they were unable to recruit neutrophils to the injured site; however, in transwell and Dunn chamber assays, *PREX1*-KO neutrophils migrated as well as their wild-type counterparts (98). Altogether, this suggests that PREX1 is a key signaling molecule in the recruitment of neutrophils to sites of inflammation, but not in the migration of individual neutrophil cells.

1.3.3. PREX1 in healthy cells

As previously described, PREX1 is a GEF that plays an important role in catalyzing the switch from inactive Rac1-GDP to active Rac1-GTP. While activation of PREX1 itself largely depends upon PIP_3 and $G\beta\gamma$ binding, PREX1 has also been shown to be activated by protein phosphatase 1α (PP1α) and inhibited by cAMP-dependent protein kinase A (PKA) (99). Once PREX1 is activated and subsequently activates Rac1, Rac1-GTP can interact with a number of downstream binding partners that drive cellular migration (91). Importantly, Rac1 activity has been shown to exercise GEF-dependent functions–while Tiam1-mediated Rac1 activation reduces cell motility, likely through IQGAP1, PREX1-mediated activation exerts the opposite effect (100). PREX1-Rac1-mediated motility has been shown to be regulated by flightless-1 homologue (FLII) which acts as a scaffold for simultaneous PREX1 and Rac1 binding and directs Rac1 activity to initiate a pro-migratory signaling cascade (100). Among Rac1's downstream effectors are the p21-

activated kinases (PAKs), PAK1, PAK2, and PAK3–serine/threonine kinases that phosphorylate and activate Lin11, Isl-1, Mec-3 kinases (LIMKs) (91). Once activated by PAKs, LIMK1 and LIMK2 phosphorylate and inactivate cofilin, a protein that normally depolymerizes actin filaments (101–103). In addition to reducing actin depolymerization, Rac1 also activates proteins that stimulate actin filament extension – in particular, the WASP-family verprolin-homologous protein (WAVE) family, and Diaphanous-related formins (DRFs) (104). After Rac1 activation, WAVE2 stimulates activity of the actin-related proteins (ARP) 2/3 complex (91). This complex directly elongates cytoskeletal filaments by serving as a nucleation site for the assembly of actin monomers on existing filaments, thus creating branched networks (105). In contrast, the DRF proteins Dia1, Dia2, and Dia3 all incorporate actin monomers onto the ends of cytoskeletal filaments, thus directly causing non-branching filament growth (104). In keeping with their roles in branched and unbranched polymerization, the WAVE complex and Dia proteins have been implicated in the formation of fan-like lamellipodia and protrusive, finger-like filopodia, respectively (104).

1.3.4. PREX1 in cancer

The importance of Rac1 to the spread of cancer is so robust that several studies have demonstrated that the metastatic potential of cancer cell lines can be increased and decreased by overexpression and knockdown of Rac1, respectively (106–108). This suggests that altering levels of PREX1 may similarly mediate glioblastoma motility via reduced activation of Rac1. Several studies have demonstrated a role for PREX1 and PREX2 in the context of cancer. In melanoma, *PREX1* is highly expressed in most primary cell lines and tumor tissue, and knockout of *PREX1* has been shown to impair melanoma invasion *in vitro* (109). Further evidence for this comes from genetic mouse models of melanoma, where deletion of *PREX1* restricts tumor metastasis and spread (109). Breast cancer cell lines and tumors also show evidence for *PREX1* overexpression

and ErbB-driven activity (110,111). PREX1 is required for the motility and tumorigenic potential of breast cancer cells, and knockdown of PREX1 has been shown to reduce tumor invasiveness *in vivo* (110). A close relative of *PREX1*, *PREX2*, is mutated in approximately 14% of melanoma cases (112). In this disease, truncating mutations to *PREX2* have been shown to enhance its Rac-GEF activity and accelerate tumor development (113).

Recently, work from our lab showed that *PREX1* was overexpressed in patient-derived glioblastoma cells, patient biopsies, and intracerebral xenografts grown in immunocompromised mice (37). Gont *et al.* demonstrated that siRNA-mediated PREX1 knockdown reduced primary glioblastoma cell motility and invasion *in vitro*, as measured by videomicroscopy and transwell invasion assays. Importantly, this behavior was phenocopied by knockdown of Rac1, consistent with both proteins acting to stimulate pro-migratory behavior (37). Tracing this pathway backwards, inhibition of PI3K and $G_{\beta\gamma}$ was reported to similarly impair cell motility.

1.3.5. Study rationale

TMs have been characterized in an *in vivo* model of glioblastoma but, to date, no *in vitro* model of these structures exists for this disease. This limits the pace at which we can study the structure and function of glioblastoma TMs and how they contribute to supporting tumor growth and invasion. Thus, we sought to characterize the first *in vitro* model of TMs using primary glioblastoma cells. Because these cells recapitulate many of the genetic and histopathological features of the original tumor, they are an accurate model upon which to base our understanding of glioblastoma TMs. Developing this model would allow future studies to expand on our findings and develop strategies to intervene with TM growth and function.

Previous studies have identified Rac1 activity as a requirement for TNT growth and extension. Rac1, and its GEF, PREX1, have also been shown to contribute to primary glioblastoma

cell motility and invasion by Gont *et al*. Considering these findings, and knowing that Rac1 has roles in both actin cytoskeleton reorganization and cell motility, it is possible that Rac1 and PREX1 contribute to TM biogenesis in an *in vitro* model of glioblastoma.

2. Hypotheses and Aims

2.1. Hypothesis #1

In vitro characterization of PriGO tumor microtubes will identify similar structural and functional properties to those observed in an *in vivo* model of glioblastoma.

2.1.1. Aims #1-4

1. Characterize TM morphology, length, and connectivity in PriGO cells.
2. Characterize mechanisms of TM formation in PriGO cells.
3. Assess the structural properties of TMs and TM-TM boundaries.
4. Assess possible functional roles for TMs in intercellular communication.

2.2. Hypothesis #2

Knockout of *PREX1* in PriGO cells will impair TM formation and growth *in vitro*.

2.2.1. Aims #5-8

5. Characterize *PREX1* and *Rac1* expression in PriGO TMs.
6. Assess the effect of PREX1 and Rac1 knockdown on TM formation.
7. Establish a *PREX1*-KO PriGO cell line using CRISPR/Cas9.
8. Characterize the effect of *PREX1*-KO on PriGO TM formation.

3. Materials & Methods

3.1. Cell culture

Primary glioblastoma (PriGO) cells were isolated from patients undergoing surgical tumor resection at The Ottawa Hospital and used throughout this study (36). Four cell lines are referred to here, derived from four different patients: PriGO7A, PriGO8A, PriGO9A, and PriGO17A. For the experiments used throughout this study, PriGO cells were between passages 10 and 25. PriGO cells were grown in monolayers on laminin-coated plates using serum-free Neurobasal A (NA) media. Media was supplemented with EGF, FGF2, B-27, and N-2 to support cellular growth. Cells were incubated in 5% O_2 and 20% CO_2 at 37˚C. Recordings and measurements described throughout this study were performed with PriGO cells plated at approximately 60% confluency.

3.2. Immunofluorescence

Prior to immunofluorescence, approximately 300,000 PriGO cells were grown on laminin-coated cover slips in 6-well dishes for 48 hours. Cells were then treated with 2mL of 4% paraformaldehyde and incubated at room temperature for 30 minutes. Cells were washed with phosphate-buffered saline (PBS) and permeated with 0.2% Triton X-100 in PBS for 10 minutes at room temperature. After washing with PBS, cover slips were blocked with 100µl of 5% normal goat serum (NGS) in PBS for one hour at room temperature. After removing the 5% NGS/PBS, cells were stained with 100µl of primary antibody in 5% NGS/PBS for one hour at room temperature. After washing, cells were stained with 100µl of secondary antibody in 5% NGS/PBS for one hour at room temperature in the dark. Cover slips were washed and mounted on +/+ microscope slides with 20µl of Prolong Gold + DAPI for visualization of the nucleus. Microscope

slides were incubated overnight in the dark at room temperature and images were acquired the following day by epifluorescence and/or confocal microscopy.

The following antibodies were used in the described experiments: PREX1 rabbit monoclonal at a concentration of 1:400 (Cell Signaling, Danvers, MA, USA), Rac1 mouse monoclonal at a concentration of 1:100 (Abcam, Cambridge, MA, USA), non-muscle myosin IIA rabbit polyclonal at a concentration of 1:500 (Sigma-Aldrich, St. Louis, MO, USA), β-tubulin mouse monoclonal at a concentration of 1:100 (ThermoFisher Scientific, Rockford, IL, USA), phalloidin at a concentration of 1:40 (Life Technologies, Burlington, ON, Canada), and Connexin 43 rabbit polyclonal at a concentration of 1:50 (Invitrogen, Camarillo, CA, USA).

3.3. Confocal microscopy

Confocal microscopy was performed using the Zeiss Laser Scanning Microscope (LSM) 800 with Airyscan. Z-stack images of PriGO cells were acquired using the 63X magnification and Zen software package.

3.4. Videomicroscopy

Approximately 30,000 PriGO8A cells were plated on laminin-coated Bioptechs delta-T dishes (Butler, PA, USA) in 1mL of complete NA media. Cells were grown for 48 hours to allow adequate time for TMs to begin forming and videomicroscopy was subsequently performed. For the duration of video acquisition, cells were maintained in a sealed chamber at 37˚C and 5% O_2. Phase contrast images were taken at 1-2.5 minute intervals for a minimum of 5 hours and a maximum of 24 hours. Images were acquired with the 10X objective of a Zeiss Axiovert 200M microscope equipped with an AxioCam HRm CCD camera (Zeiss, Göttingen, Germany). TM

lengths were quantified manually using Fiji software; an example is shown in Supplementary Figure 1. TM motility was also quantified using Fiji with the MTrackJ Fiji plugin.

3.5. Transmission Electron Microscopy (TEM)

PriGO8A cells were cultured on a glass light microscope slide and processed in situ. The slide with monolayer was immersed in 2.5% (sodium cacodylate buffered) glutaraldehyde for one hour at 4˚C, transferred through a 3X rinse in 0.05M Sodium Cacodylate buffered to pH 7.2. Next, the slide was immersed in 2% Osmium Tetroxide for 1 hour, followed by rinses in water and a dehydration schedule through graded ethanols (50%, 70% through several changes in absolute EtOH). After a final dehydration in acetone, several drops of Spurr's resin were placed on the area of interest and the slide inverted on a BEEM capsule slightly over-filled with Spurr's resin, ensuring contact with resin and the slide surface and placed in a 70˚C oven overnight. After polymerization, the slide with inverted capsule was lightly heated on a hot plate for several seconds and the block eased off the slide. The block was thin sectioned for electron microscopy and the sections stained with uranyl acetate followed by lead citrate and screened on a Hitachi H-7100 transmission electron microscope at 75Kv.

3.6. Mitochondria labelling

PriGO8A cells were incubated for 30 minutes with 100nM MitoTracker Red FM diluted in complete NA media, followed by three washes with PBS and addition of NA media. Mitochondrial labelling could be detected immediately after incubation and washing by EVOS microscopy or videomicroscopy and persisted for up to two days. After incubation, labelled cells were passaged and plated in delta-T dishes with PriGO8A-GFP cells for videomicroscopy.

3.7. RNA interference

RNA duplexes targeting Rac1 and PREX1 were purchased from Dharmacon (Lafayette, CO, USA) and had the following sense strand sequences: siRac1a (UAAGGAGAUUGGUGCUGUA), siRac1b (UAAAGACACGAUCGAGAAA), siPREX1a (GAGAUGAGCUGCCCUGUGA), and siPREX1b (GAAAGAAGAGUGUCAAAUC). Non-targeting siRNA controls were also purchased from Dharmacon. To prepare the siRNA complex for transfection, oligofectamine and Opti-MEM were first mixed at a ratio of 4µl to 11µl, respectively, per well, and incubated at room temperature for 10 minutes. Separately, siRNA duplexes were mixed with Opti-MEM to a final volume of 185µl per well. Calculations were performed so that the concentration of siRNA duplex in the final 1ml volume added to each well would be 20nM. 15µl of the oligofectamine and Opti-MEM mixture prepared previously were mixed with each 185µl siRNA mixture and incubated at room temperature for 20 minutes. PriGO8A cells were then washed with PBS and 800µl of Opti-MEM was added to each well. The 200µl siRNA mixtures were then added drop-wise to their respective well. Cells were incubated for 4 hours, after which 2ml of complete NA media were added. Cells were then incubated for 48 hours and then washed and replenished with complete NA media only. Subsequent experiments assessed the effect of siRNA-mediated knockdown on TM formation and growth.

3.8. Lentivirus transduction

To induce constitutive GFP or mCherry expression, PriGO8A cells were transduced with either pLenti-CMV GFP Puro (Addgene Plasmid #17448) or pLV-mCherry (Addgene Plasmid #36084), respectively. Cells transduced with pLenti-CMV GFP Puro were subsequently incubated in 0.5µg/ml of puromycin for four days, with antibiotics refreshed every second day, to select for

PriGO8A cells that expressed GFP. Cells of each population were subsequently co-cultured for 48 hours to allow sufficient time for the formation of TMs and were then recorded by videomicroscopy to determine whether protein exchange could be detected.

For the lentiviral knockout of GFP, lentiCRISPR EGFP sgRNA (Addgene Plasmid #51764) was used. This virus contains a puromycin selection cassette and expresses Cas9 protein and an EGFP-targeting synthetic sgRNA. PriGO8A cells with constitutive GFP expression were cultured in a 6-well plate and incubated with 1ml of lentiCRISPR EGFP virus for 4 hours, after which 1ml of complete NA media was added to the solution. 24 hours later, the virus-containing solution was replaced with 2ml of fresh media. After 24 hours, cells were incubated in 1µg/ml of puromycin to select for those that were successfully transduced by the lentiCRISPR EGFP virus. Puromycin selection was continued for four days, and cells were then imaged by EVOS microscopy to assess changes in GFP expression.

3.9. Transfection

After lentiCRISPR transduction, lipofection-mediated CRISPR/Cas9 was tested. First, approximately 200,000 PriGO8A cells were plated in each well of a 6-well plate and left to plate down overnight. These experiments began with two crRNAs targeting *PREX1* (sequence #1: TTGCAGAGCTGCATGCTTCT, PAM #1: GGG, located on exon 5 of *PREX1*; sequence #2: TATCGCTTCCGCTACGACGA, PAM #2: TGG, located on exon 12 of *PREX1*; Dharmacon). Subsequent experiments were performed using the first crRNA that targeted exon 5 because it was determined to have higher on-target specificity and lower off-target activity by the Deskgen Guide Picker online tool. To begin preparing the CRISPR complex, 1X siRNA buffer was prepared by combining 800µl sterile PBS and 200µl 5X siRNA buffer. crRNA:tracrRNA oligos were then

prepared by mixing 1µl 100µM crRNA, 1µl 100µM tracrRNA, and 98µl 1X siRNA buffer per well. This solution was heated at 95˚C for 5 minutes and then cooled on the benchtop to room temperature. To produce the ribonucleoprotein (RNP) complex for each well, 50µl 1µM complexed crRNA:tracrRNA oligos, 20µl 1µM Cas9 nuclease, and 300µl Opti-MEM were all mixed together. The solution was then incubated at room temperature for 5 minutes. For each well, 5µl lipofectamine and 1625µl Opti-MEM were mixed together and incubated at room temperature for 5 minutes. The lipofectamine solution was then mixed with 370µl of RNP complex to achieve a final RNP concentration of 25nM, and the solution was incubated for 20 minutes at room temperature. 2ml of transfection complexes was added to each well of a 6-well dish. 48 hours later, DNA was extracted from cells to be assessed for mutations by the T7EI assay (described below).

3.10. CRISPR/Cas9 electroporation

Electroporation-based delivery of CRISPR/Cas9 components was performed and adapted from IDT DNA Technologies. First, an electroporation enhancer (Alt-R Cas9 Electroporation Enhancer, IDT DNA Technologies) was prepared to increase the efficiency of electroporation. 1.08µl of 100µM stock electroporation enhancer was combined with 8.92µl of water to form a 10.8µM working solution. For the crRNA:tracrRNA duplex, a crRNA sequence targeting exon 2 of *PREX1* was used (Dharmacon; sequence: CGTTCTGCCGGATGCGATGC, PAM: AGG). This was combined with tracrRNA-ATTO 550 (IDT DNA Technologies) to a final duplex concentration of 44µM (e.g. 4.4µl 100µM crRNA, 4.4µl 100µM tracrRNA, 1.2µl water) to form the complete guide RNA complex. The complex was then heated at 95˚C for 5 minutes. To form the Cas9 solution, for each well, 0.3µl of 61µM Cas9 nuclease stock solution was combined with 0.2µl of Resuspension Buffer R. To form the crRNA:tracrRNA:Cas9 complex, for each well, 0.5µl

of crRNA:tracrRNA complex was combined with 0.5µl of diluted Cas9 nuclease and incubated for 20 minutes at room temperature. PriGO8A cells, grown to 70-80% confluence, were then resuspended in Resuspension Buffer R to 500,000 cells per well. For each well, the following complex was prepared: 1µl crRNA:tracrRNA:Cas9 complex, 9µl cell suspension, and 2µl of 10.8µM electroporation enhancer. To prepare the Neon Transfection System for electroporation, the Neon Tube was filled with 3ml of Electrolytic Buffer (E Buffer if using a 10µl tip; E2 Buffer if using a 100µl tip) and inserted into the Neon Pipette Station. A Neon Tip was inserted into the Neon Pipette and 10µl of the 12µl solution available for each well was drawn into the tip, taking care to avoid air bubbles. The Neon Pipette and Tip were inserted into the Pipette Station. The following electroporation parameters were used: 1050V, 30ms, and 2 pulses. After electroporation, cells were immediately plated on a laminin-coated 6-well plate, incubated in normal PriGO culture conditions, and ATTO 550 fluorescence was verified 24 hours later by EVOS microscopy. Cells were passaged once to ensure that they maintained their normal rate of proliferation and, two weeks after the first round of electroporation, a second round was performed on the same cells with the same experimental set-up and electroporation parameters. A T7EI assay (described below) was performed on the twice-electroporated cells to validate the presence of *PREX1*-targeted mutations. Immunofluorescence was performed to confirm loss of PREX1 protein production. These cells (hereafter referred to as *PREX1*-KO PriGO8A cells) were subsequently carried and characterized for the motility and TM growth.

3.11. T7 Endonuclease I (T7EI) assay

The T7EI assay was performed after CRISPR/Cas9 to validate the presence of mutations inserted at the target *PREX1* site. After performing PCR for the target region, amplified DNA was

purified according to the QIAquick PCR Purification Kit handbook and the amount of DNA was quantified with a NanoDrop Microvolume Spectrophotometer. To form heteroduplexed DNA, assembly required 200ng of purified PCR product, 2µl of 10X NEBuffer 2, and the addition of nuclease-free water to 19µl. PCR products were separated and annealed together under the following conditions: 10 minutes at 95˚C, –2˚C/second from 95˚C to 85˚C, –0.1˚C/second from 85˚C to 25˚C, and a hold at 25˚C. After forming heteroduplexes, 19µl of heteroduplexed DNA was incubated with 1µl of the T7EI enzyme (New England BioLabs, Ipswich, MA, USA) for 25 minutes at 37˚C. The digested DNA was then run on a 1.5% agarose gel for approximately 1 hour at 100V to detect parent and fragmented bands. Alongside the digested DNA, two controls were run: a PCR product control, and a heteroduplexed, undigested PCR product control.

3.12. Statistical analyses

Statistical analyses were performed using the GraphPad Prism program. To compare two groups, unpaired two-tailed t-tests were used. Multiple groups were compared using a two-way Analysis of Variance (ANOVA) test with a Tukey post-hoc analysis. Graphs show the mean and standard error of the mean (SEM) for each collection of data points. P values are represented as * < 0.05, ** < 0.01, *** < 0.001, and **** < 0.0001.

4. Results

4.1. Aim 1: Characterize TM morphology, length, and connectivity in PriGO cells.

4.1.1. TMs connect PriGO cells in vitro

TMs were characterized in primary glioblastoma (PriGO) cells that were isolated from patients undergoing surgical tumor resection at The Ottawa Hospital. Four PriGO cell lines were

grown on laminin-coated plates at 37˚C in 5% O_2 and 20% CO_2. Importantly, the presence of laminin allows PriGO cells to grow as a monolayer, extend cellular processes, and establish TMs with other cells. Laminin has also been shown to maintain glioblastoma cells in a stem cell-like state *in vitro* (114,115). However, previous work with *in vitro* models of glioblastoma have demonstrated that collagen, hyaluronan, and Matrigel can also be used as 2D or 3D scaffolds for cellular growth (116–118). Without an appropriate scaffold, glioblastoma cells grow as individual neurospheres that do not demonstrate the same tendency to form intercellular contacts (36). Thus, laminin was necessary to characterize a cell culture model of glioblastoma TMs. TMs were defined as cellular extensions that form physical contacts between PriGO cells, distinguishing them from filopodia-like protrusions that form and retract without bridging cells (Figure 1A-C). Consistent with previous reports, TMs formed above the culture plate surface and did not contact the substrate, as demonstrated by a 3D reconstruction of PriGO cells imaged by confocal microscopy (Figure 1D-E). In some cases, TMs were also seen to pass over other TMs or nearby cells, further demonstrating their non-adherence to the plate.

4.1.2. TM length and connectivity

PriGO cells obtained from four different patients (referred to as 7A, 8A, 9A, and 17A) were characterized for their TM length and connectivity. Supplementary Figure 1 shows an example of the TM length quantification process. TM connectivity was defined as the percent of cells connected by TMs in culture, and determined by calculating the proportion of connected cells in multiple fields of view under the microscope. Comparison of TM lengths showed that PriGO9A cells form the shortest connections, with a mean length of 61.60µm, while PriGO17A cells formed the longest TMs with a mean length of 82.77µm (Figure 2A; $n \geq 70$ TMs measured per PriGO cell line). PriGO7A and PriGO8A cells reached intermediate mean lengths of 70.82µm and 65.62µm,

respectively. Interestingly, all PriGO cells were capable of forming TMs as short as 18μm and extending over 200μm in length. The longest connections observed between cells were still considerably shorter than those seen in glioblastoma *in vivo* (71).

The percent of cells connected by TMs also varied across PriGO cultures obtained from different patients; PriGO8A cells showed the highest percentage of connectivity, while PriGO7A cells showed the least (68.12% vs. 36.22%, respectively; Figure 2B). PriGO9A and PriGO17A cells exhibited an intermediate degree of connectivity, with TMs forming between 53.41% and 44.26% of cells, respectively. A similar degree of variability was observed in the percent of cells connected by ≥ 1 TM to other cells in culture (Figure 2C). In this regard, PriGO8A cells were most often connected by 1 TM and least connected by 3 or more TMs compared to other cell lines; a pattern also seen in PriGO9A and PriGO17A cells. In contrast, of the PriGO7A cells that formed TMs, three-quarters formed 2 TMs and the remainder were almost equally likely to form 1 or 3+ TMs.

Further TM characterization (described in the results below) was only performed on PriGO8A cells, which show an intermediate TM length and high degree of connectivity. This cell line was chosen because it has been thoroughly characterized by previous studies from our lab (36–38).

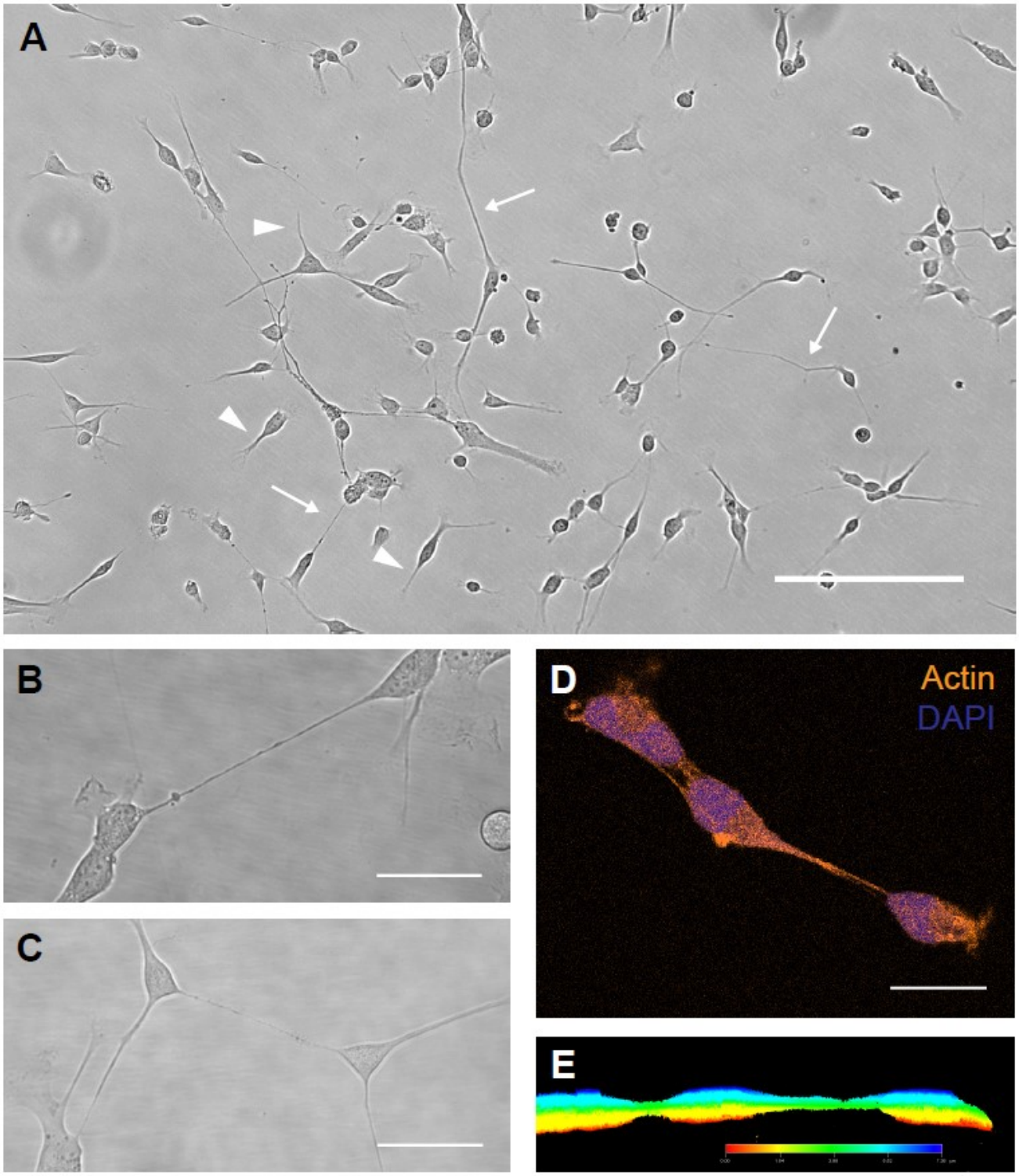
A
B
C
D
Actin
DAPI
E

Figure 1. PriGO cells form physical contacts *in vitro*, termed tumor microtubes (TMs).

A. Representative images of TMs observed in PriGO8A cells grown on laminin-coated dishes. → indicates TMs connecting two PriGO8A cells together; ► indicates filopodia-like projections that do not connect cells. Scale bar = 200μm. **B-C.** High-magnification images of TMs observed in PriGO8A cells. Scale bars = 50μm. **D-E.** TMs form above the substrate surface and do not adhere to the plate as demonstrated by 3D reconstruction of z-stack images acquired by confocal microscopy. Scale bar = 20μm.

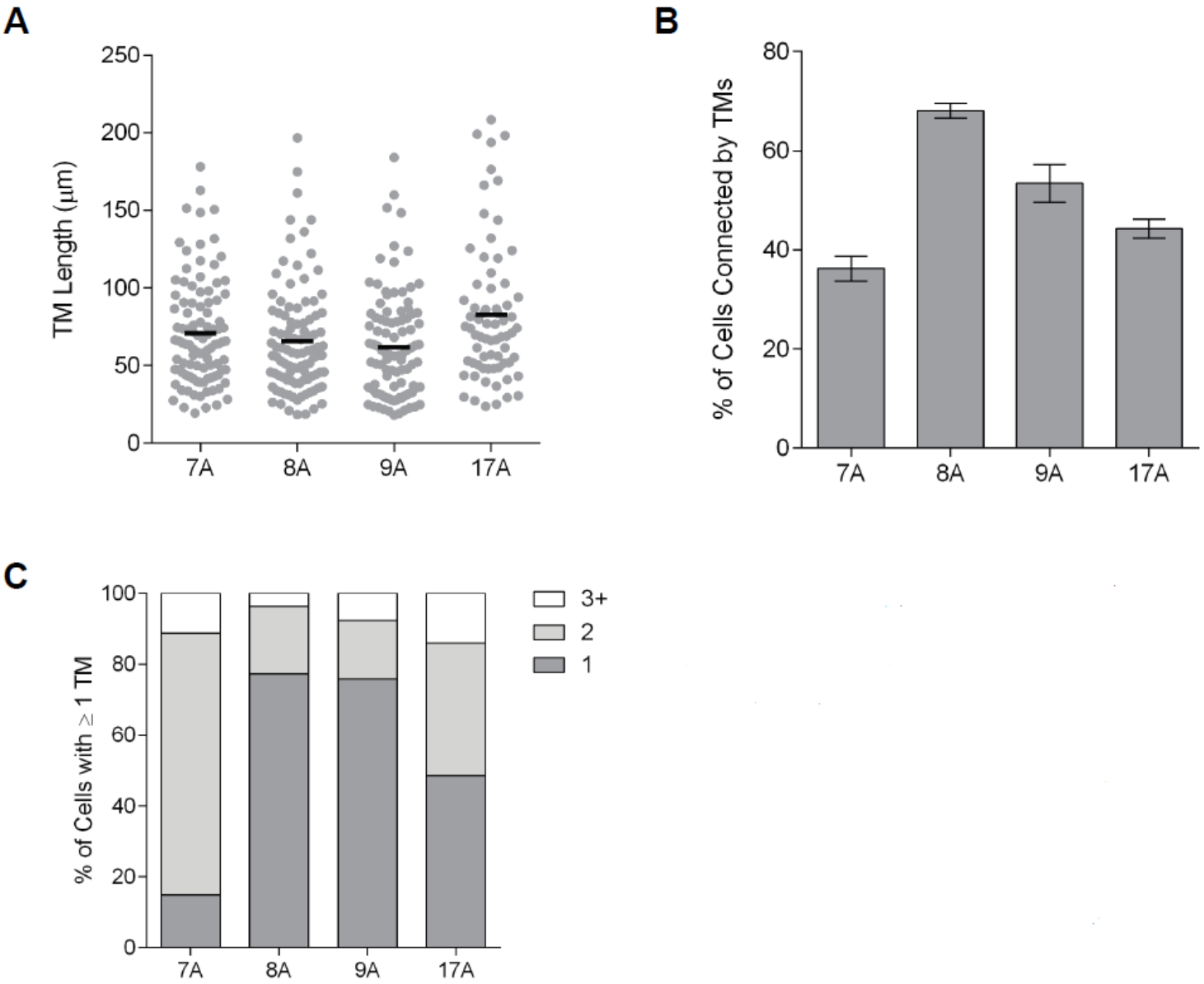
A
TM Length (µm)
250
200
150
100
50
0
7A
8A
9A
17A
B
% of Cells Connected by TMs
80
60
40
20
0
7A
8A
9A
17A
C
% of Cells with ≥ 1 TM
100
80
60
40
20
0
7A
8A
9A
17A
3+
2
1

Figure 2. PriGO cells from different patients exhibit TM heterogeneity.

A. TM lengths were quantified in PriGO cells obtained from four different patients and cultured *in vitro* (n = 100 TMs measured per PriGO cell line). Cells were plated in T-25 flasks and brightfield images were acquired by EVOS microscopy 48 hours later when cells were at approximately 60% confluency. At this confluency, all visible TMs were included in quantifications. TM measurements were aggregated from 8-10 fields of view per cell line. **B.** The percent of cells connected by TMs *in vitro* varies in different PriGO cell lines. The images used to obtain the quantification panel A were subsequently used for quantifying PriGO cell connectivity. **C.** PriGO cells from each patient were characterized for the number of TMs formed by individual cells, categorized as 1, 2, or 3+ TMs per cell. Individual cells were rarely seen forming more than 4 TMs.

4.2. Aim 2: Characterize mechanisms of TM formation in PriGO8A cells.

4.2.1. TMs form by two mechanisms in vitro

Videomicroscopy of PriGO8A cells demonstrated instances of both cell dislodgement and ADP mechanisms occurring *in vitro* (representative examples of images acquired by videomicroscopy shown in Figure 3A-B). Analysis of 72 TM formation events indicated that PriGO8A TMs preferentially form using the cell dislodgement mechanism compared to the ADP mechanism (60% vs. 40% of events, respectively; Figure 3C). Of note, TM events counted towards the cell dislodgement mechanism do not include instances of cells undergoing mitosis and retaining a TM between each other following cytokinesis.

The TM lifetime was then defined as the point at which a TM was first established between two cells until it first disconnected from either cell in the pairing. Videomicroscopy was performed for up to 24 hours, with images captured every 1-2.5 minutes, and identified an overall mean lifetime of 53.15 minutes. Classifying events according to their formation mechanism revealed that ADP-derived TMs had a significantly longer mean lifetime than their dislodgement counterparts at 72.93 minutes compared to 39.80 minutes, respectively (Figure 3D). In both mechanisms, TMs disconnected after as little as a few minutes but were able to persist for over 3 hours in some cases. For each recorded TM event, the maximum length reached was also quantified, indicating the maximum distance over which cells remained connected *in vitro*. TMs forming according to the ADP mechanism reached significantly greater lengths than TMs derived from dislodgement events (mean = 152.9µm vs. 104.3µm, respectively; Figure 3E). In rare instances, TMs were even seen connecting cells 300-400µm apart.

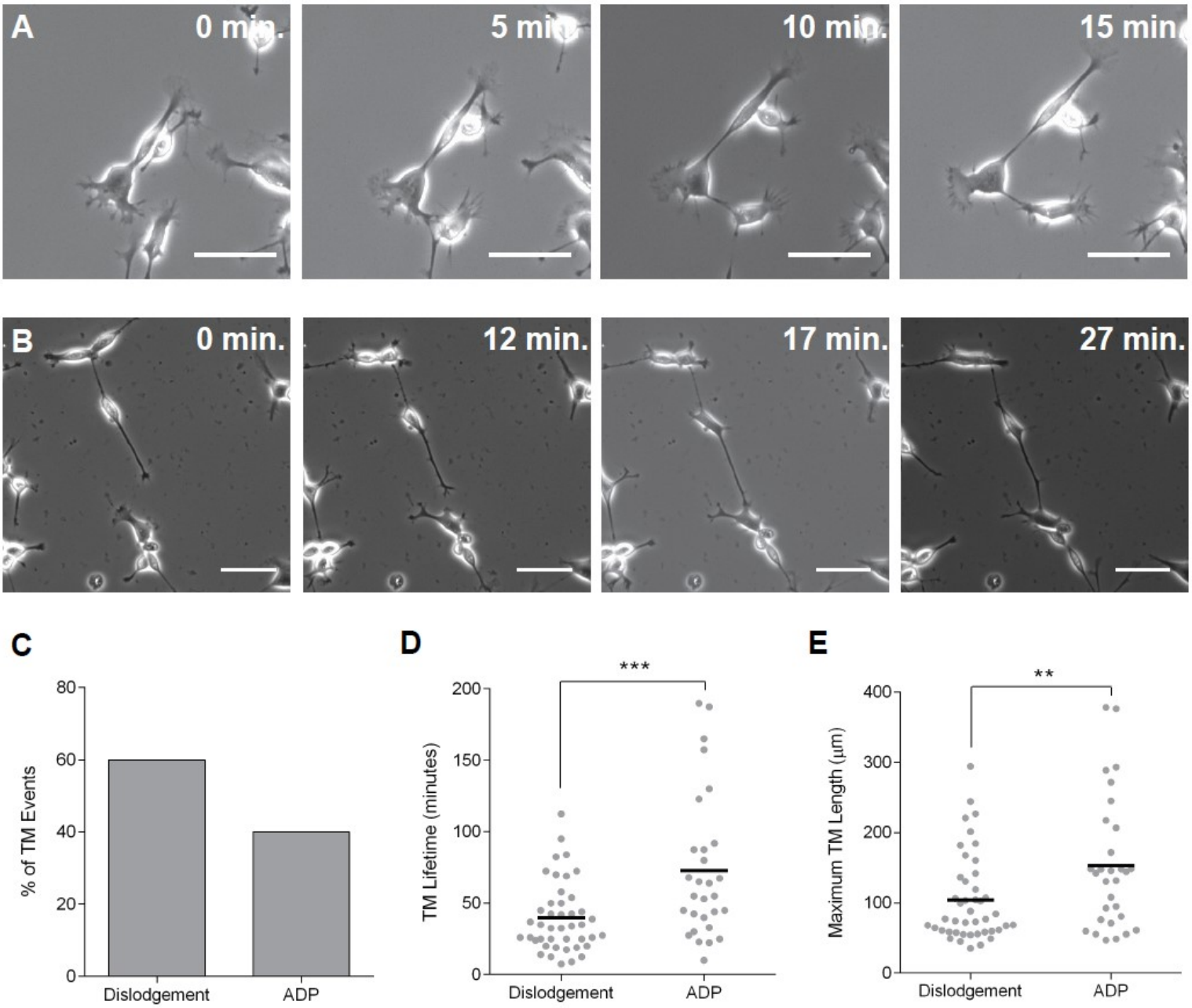
A
0 min.
5 min.
10 min.
15 min.
B
0 min.
12 min.
17 min.
27 min.
C
% of TM Events
80
60
40
20
0
Dislodgement
ADP
D
TM Lifetime (minutes)
***
200
150
100
50
0
Dislodgement
ADP
E
Maximum TM Length (µm)
**
400
300
200
100
0
Dislodgement
ADP

Figure 3. PriGO8A TMs form by two different mechanisms *in vitro.*

A-B. Representative examples of the processes by which cell dislodgement- and ADP-derived TMs form, respectively, between PriGO8A cells. Scale bars = 100μm. **C.** PriGO8A TMs show preference for forming via the cell dislodgement mechanism (n = 72 events observed in 9 videos). **D.** Analysis of 72 PriGO8A TM events identified differences in the mean lifetime of dislodgement- and ADP-derived TMs. **E.** PriGO8A TMs are capable of reaching different maximum lengths depending on their mechanism of formation. A significant difference was also observed in the mean maximum TM length for each mechanism.

4.3. Aim 3: Assess the structural properties of TMs and TM-TM boundaries.

4.3.1. Immunofluorescence for TM structural proteins

Immunofluorescence performed on PriGO8A cells identified a number of structural proteins found within TMs. Similar to the observations of Osswald *et al.* (2015), TMs were positive for actin, β-tubulin, and non-muscle myosin IIA (Figure 4A-C). Immunofluorescence performed on PriGO9A and PriGO17A cells also showed evidence for actin and β-tubulin in TMs of these cell lines (Supplementary Figure 2). This suggests that the structural contents of PriGO cells cultured *in vitro* mimic those reported *in vivo.*

4.3.2. Characterization of the TM-TM boundary

Ultrastructural analysis of TMs was performed using transmission electron microscopy (TEM) to ascertain whether PriGO8A cells *in vitro* recapitulate the same gap junction-containing phenotype as cells *in vivo*. Increased structural densities characteristic of gap junction proteins were observed at the boundaries of projections from separate PriGO8A cells and were associated for several hundred nanometers (Figure 5A-F). In some cases, the protein densities observed on paired cells were separated by a nanometer-scale gap. This provides preliminary evidence that gap junctions may form at the boundary of two TMs or the boundary of a TM and cell body.

Subsequently, immunofluorescence was performed on PriGO8A cells for gap junction-specific protein Cx43. This labelled TMs and frequently stained discrete patches along the length of TMs, possibly detecting the point of physical contact between cells. (Figure 6A-B). This, combined with the TM results presented above, provides further evidence for the presence of gap junctions at the TM-TM boundary between cells.

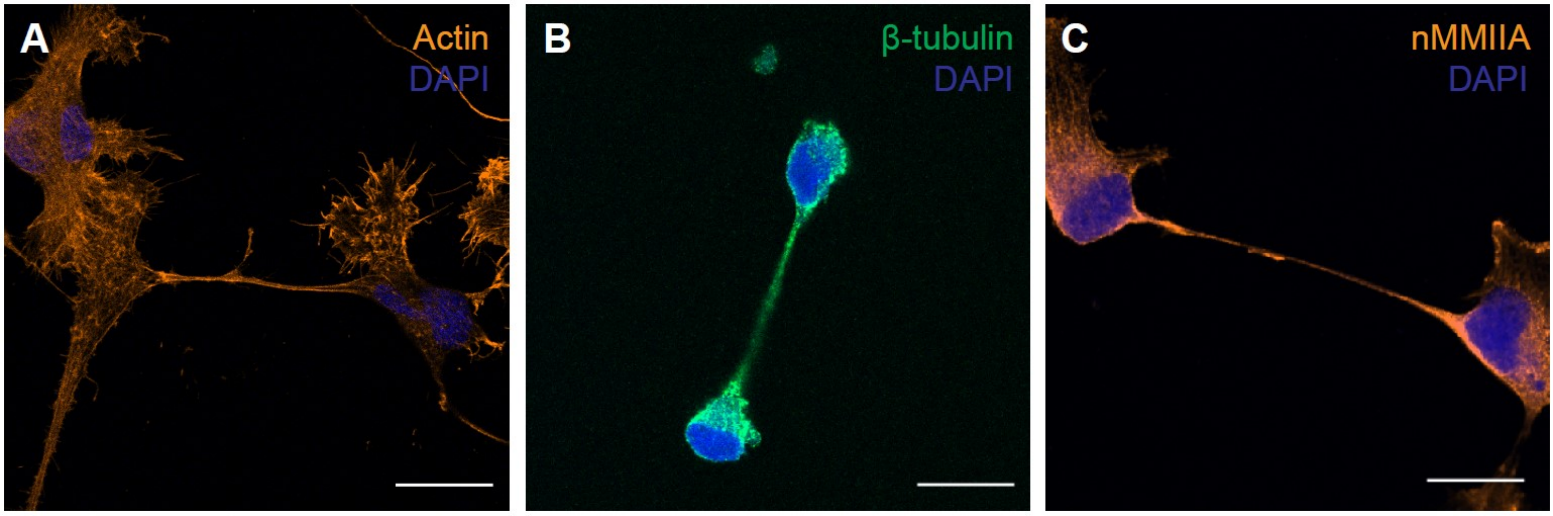
A
Actin
DAPI
B
β-tubulin
DAPI
C
nMMIIA
DAPI

Figure 4. The structural proteins that characterize PriGO8A TMs are similar to those observed *in vivo* by Osswald *et al.*

A-C. Representative images of actin, β-tubulin, and non-muscle myosin IIA (nMMIIA), respectively, found within the length of PriGO8A TMs *in vitro*. 63X images were acquired by confocal microscopy. Scale bars = 20μm.

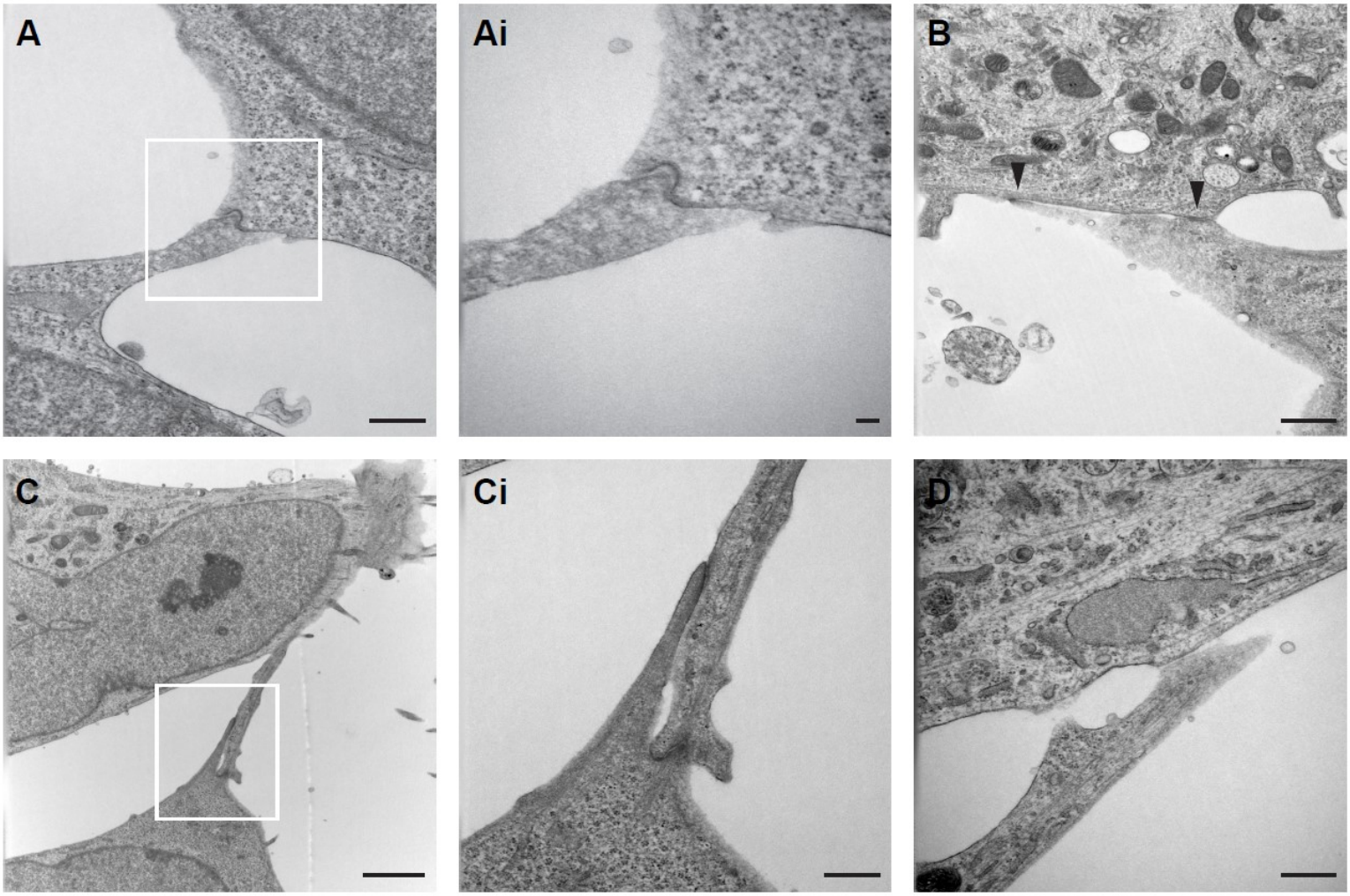
A
Ai
B
C
Ci
D

Figure 5. Transmission electron microscopy of the TM-TM boundary.

A. Transmission electron micrograph showing the boundary of two PriGO8A cells and a presumptive gap junction. Scale bar = 500nm. **Ai.** High magnification image of inset shown in A. Scale bar = 100nm. **B.** Transmission electron micrograph showing two points of contact between two neighboring cells, as evidenced by regions of high density protein, indicated by ►. Scale bar = 500nm. **C.** Transmission electron micrograph of two overlapping TMs with multiple points of contact. Scale bar = 2µm. **Ci.** High magnification image of inset shown in C. Scale bar = 500nm. **D.** Transmission electron micrograph of the boundary between two adjacent PriGO8A cells. Scale bar = 500nm.

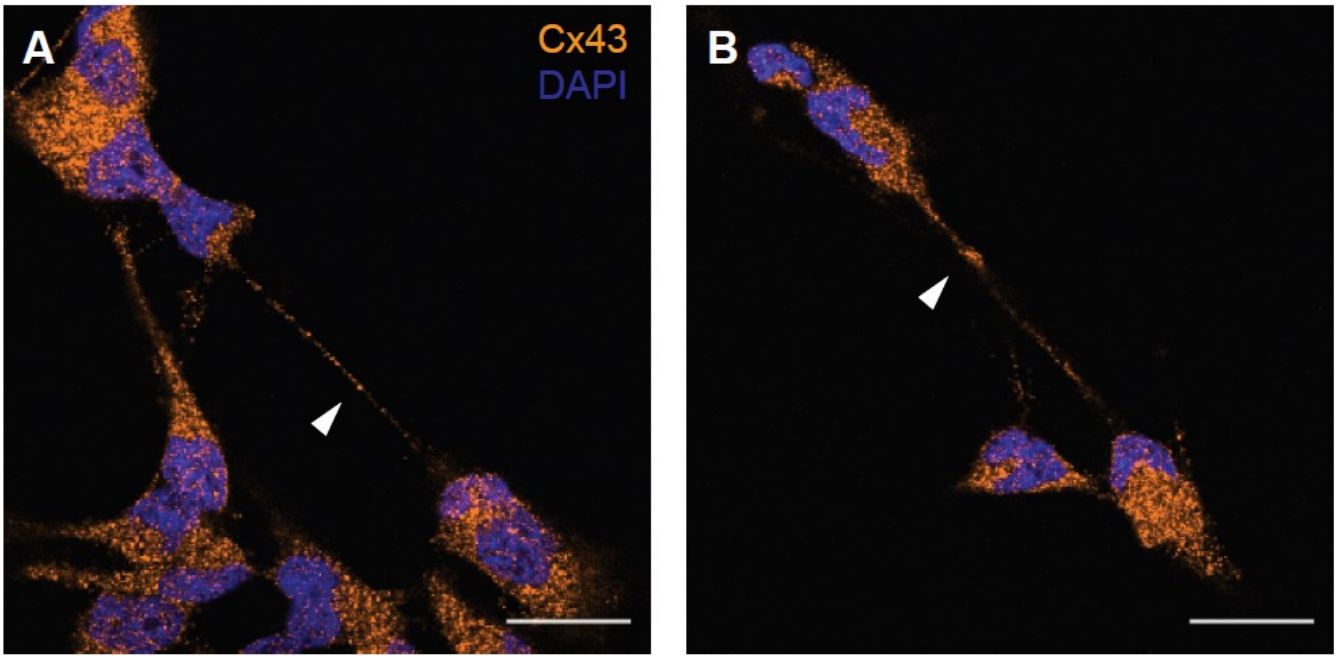
A
Cx43
DAPI
B

Figure 6. Immunofluorescence for gap junction protein Connexin 43 positively labels PriGO8A TMs.

A-B. Connexin 43 (Cx43) staining in PriGO8A cells positively labels TMs connecting cells and identifies distinct patches of staining along the length of the TM (indicated by ►). This closely resembles the typical pattern of staining observed in other cell lines that stain positively for Cx43 (described further in Discussion). Dense patches of staining along the length of TMs could indicate sites of physical contact between TMs originating from different cells. Overall, this staining pattern further supports the likelihood of gap junctions separating PriGO8A cells. Scale bars = 20μm.

4.4. Aim 4: Assess possible functional roles for TMs in intercellular communication.

4.4.1. Assessment of mitochondrial exchange

To determine how permissive PriGO8A TMs were for intercellular communication, we first assessed whether mitochondria could be transferred between cells. Mitochondria in a population of PriGO8A cells were labelled with MitoTracker Red FM and cells were co-cultured with a population of GFP-expressing PriGO8A cells. Videomicroscopy recordings showed that mitochondrial labelling was concentrated in the cell body and evidence from TEM micrographs shows mitochondria in the length of cellular projections (Supplementary Figure 3). However, no overlapping fluorescence was detected in any of the recordings made, suggesting that intercellular mitochondrial exchange does not occur between PriGO8A cells (n = 4 videos; Figure 7A).

4.4.2. Assessment of GFP and mCherry exchange

To determine whether TM size restricts the passage of large, but not small, cellular cargo, two populations of PriGO8A cells were transduced with lentivirus to constitutively express either GFP (MW = 27kDa) or mCherry (MW = 28.8kDa) and co-cultured for 24 hours. Cells were then recorded by videomicroscopy for 5-24 hours and, in all cases (n = 4 videos), GFP and mCherry remained in their respective host cell despite being expressed along the length of TMs. No protein transfer was observed to occur between cells, irrespective of TM connectivity. This was confirmed for both the cell dislodgement and ADP formation mechanisms (Figure 7B-C). Supplementary Figure 4 shows an example of two cells connected by an ADP-derived TM with protrusions originating from both cells. Overall, the inability of TMs to serve as a conduit for intercellular protein and mitochondrial exchange is likely to be due to the structural properties of the TM's cell-cell boundary.

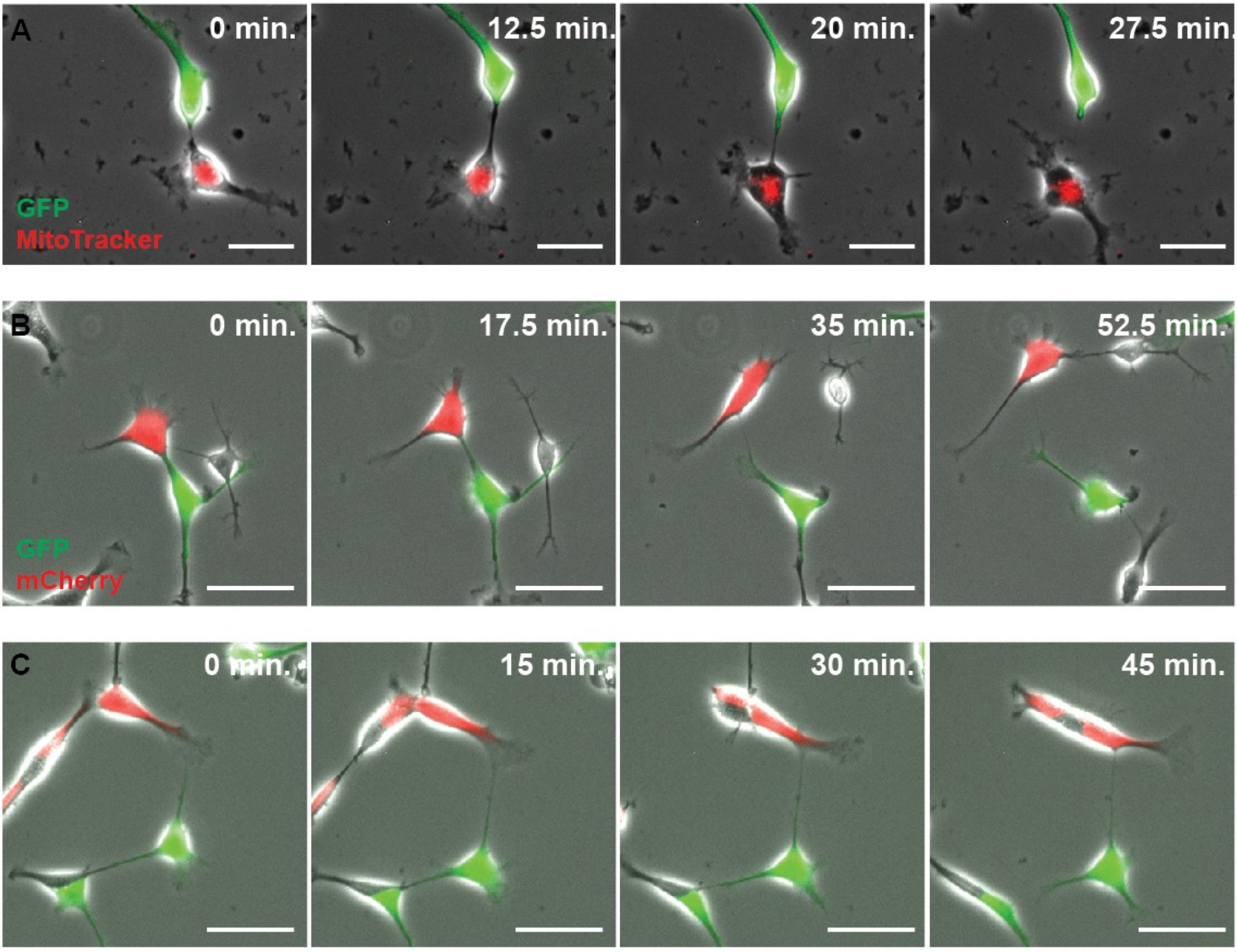
A
0 min.
12.5 min.
20 min.
27.5 min.
GFP
MitoTracker
B
0 min.
17.5 min.
35 min.
52.5 min.
GFP
mCherry
C
0 min.
15 min.
30 min.
45 min.

Figure 7. PriGO8A TMs do not facilitate the exchange of mitochondria or GFP and mCherry.

A. PriGO8A TMs cannot be used to transfer mitochondria. Co-cultured populations of cells labelled with either GFP (green) or MitoTracker Red FM (red) retained their fluorescence after up to 24 hours; no overlap was observed (n = 4 videos). Representative images of two cells forming a TM via the cell dislodgement mechanism and not exchanging mitochondria after separating. Scale bars = 50μm. **B-C.** PriGO8A TMs cannot be used for the intercellular transfer of proteins such as GFP and mCherry. Representative images of a cell dislodgement-derived TM and ADP-derived TM, respectively, with lifetimes close to the mean, are shown. No overlap of fluorescence was detected after up to 24 hours of co-culture, suggesting that protein was not being exchanged between cells (n = 6 videos). Scale bars = 100μm.

4.5. Aim 5: Characterize PREX1 and Rac1 expression in PriGO8A TMs.

4.5.1. Immunofluorescence for PREX1 and Rac1

To determine whether PREX1 and Rac1 could be involved in TM formation, their expression was first characterized in PriGO8A cells by immunofluorescence (Figure 8A-D). TMs stained positively for both proteins, with PREX1 exhibiting a more punctate distribution pattern than Rac1. Importantly, this represents the first evidence for the expression of both proteins in glioblastoma TMs.

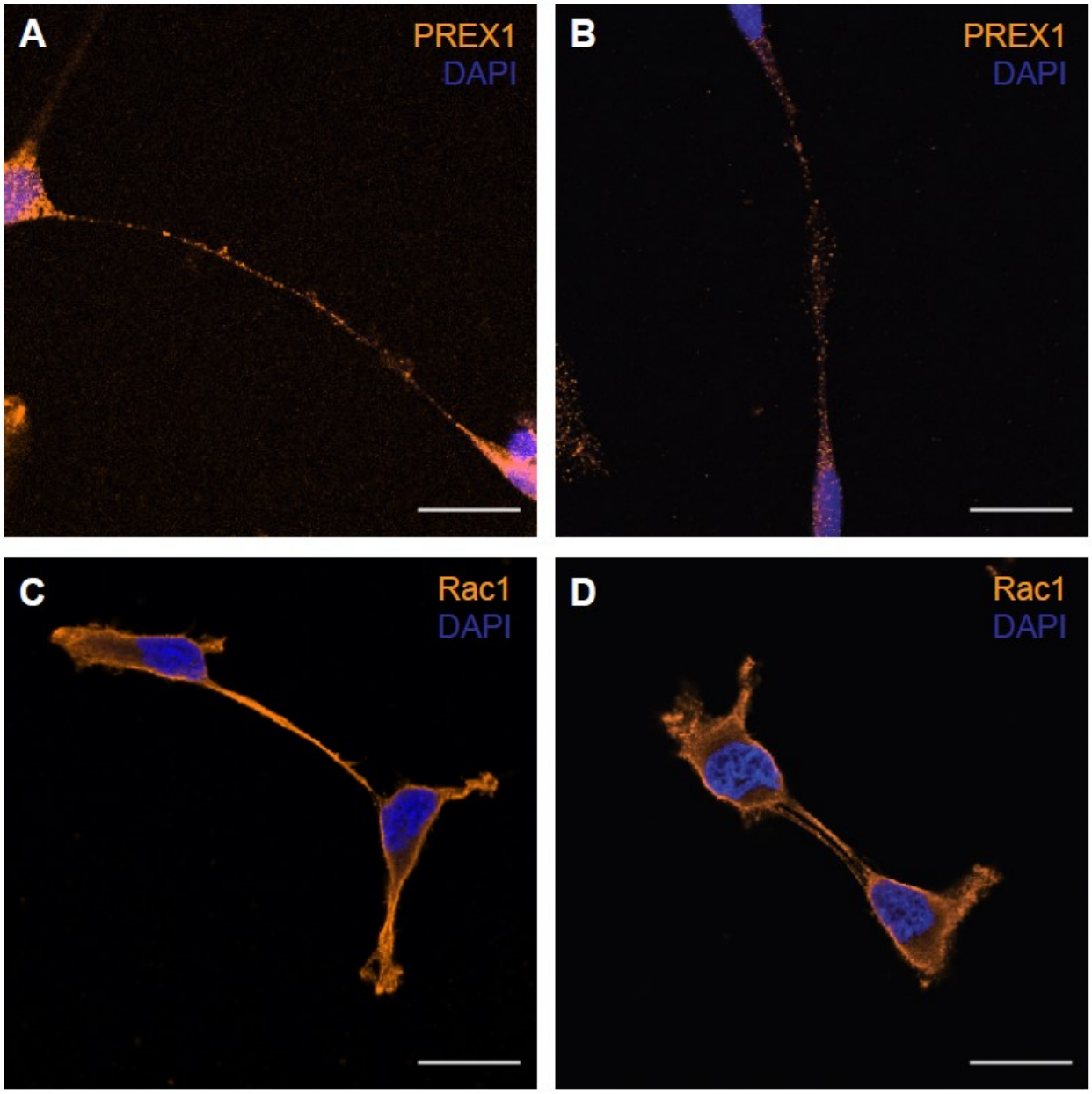
A
PREX1
DAPI
B
PREX1
DAPI
C
Rac1
DAPI
D
Rac1
DAPI

Figure 8. PREX1 and Rac1 are expressed in PriGO8A TMs *in vitro.*

A-B. PREX1 exhibits a punctate staining pattern in PriGO8A TMs but is observed throughout the length of these structures. Scale bars = 20μm. **C-D.** PriGO8A cells stain positively for Rac1, which has a more homogenous distribution pattern throughout TMs. Scale bars = 20μm. All images were acquired by confocal microscopy at 63X magnification.

4.6. Aim 6: Assess the effect of PREX1 and Rac1 knockdown on TM formation.

4.6.1. Knockdown of PREX1 and Rac1

To assess possible functional roles for PREX1 and Rac1 in TM formation and growth, siRNA knockdowns were subsequently performed. PriGO8A cells were incubated with one of two siRNA duplexes targeting either PREX1 or Rac1. After 48 hours, cells were imaged by EVOS microscopy and protein was extracted for Western blot analysis. Analysis of the resulting populations showed that mock- and si2-transfected cells had comparable TM lengths and connectivity to the analysis shown in Figure 2, so were likely unaltered by the experiment conditions. However, siRac1- and siPREX1-treated cells all exhibited significant reductions in TM length, as shown in Figure 9A-F (si2 vs. siRac1a vs. siRac1b, 54.41µm vs. 39.16µm vs. 39.64µm; si2 vs. siPREX1a vs. siPREX1b, 62.19µm vs. 44.77µm vs. 46.28µm). A similar reduction was observed in the percent of connected cells (si2 vs. siRac1a vs. siRac1b, 59.17% vs. 41.67% vs. 33.33%; si2 vs. siPREX1a vs. siPREX1b, 56.67% vs. 37.50% vs. 35.00%). This presents the first evidence that PREX1 and Rac1 are involved in glioblastoma TM formation. To confirm this finding for PREX1, and to determine whether complete loss of PREX1 protein has more deleterious effects on motility and TM growth, we performed a CRISPR/Cas9-based knockout of *PREX1*.

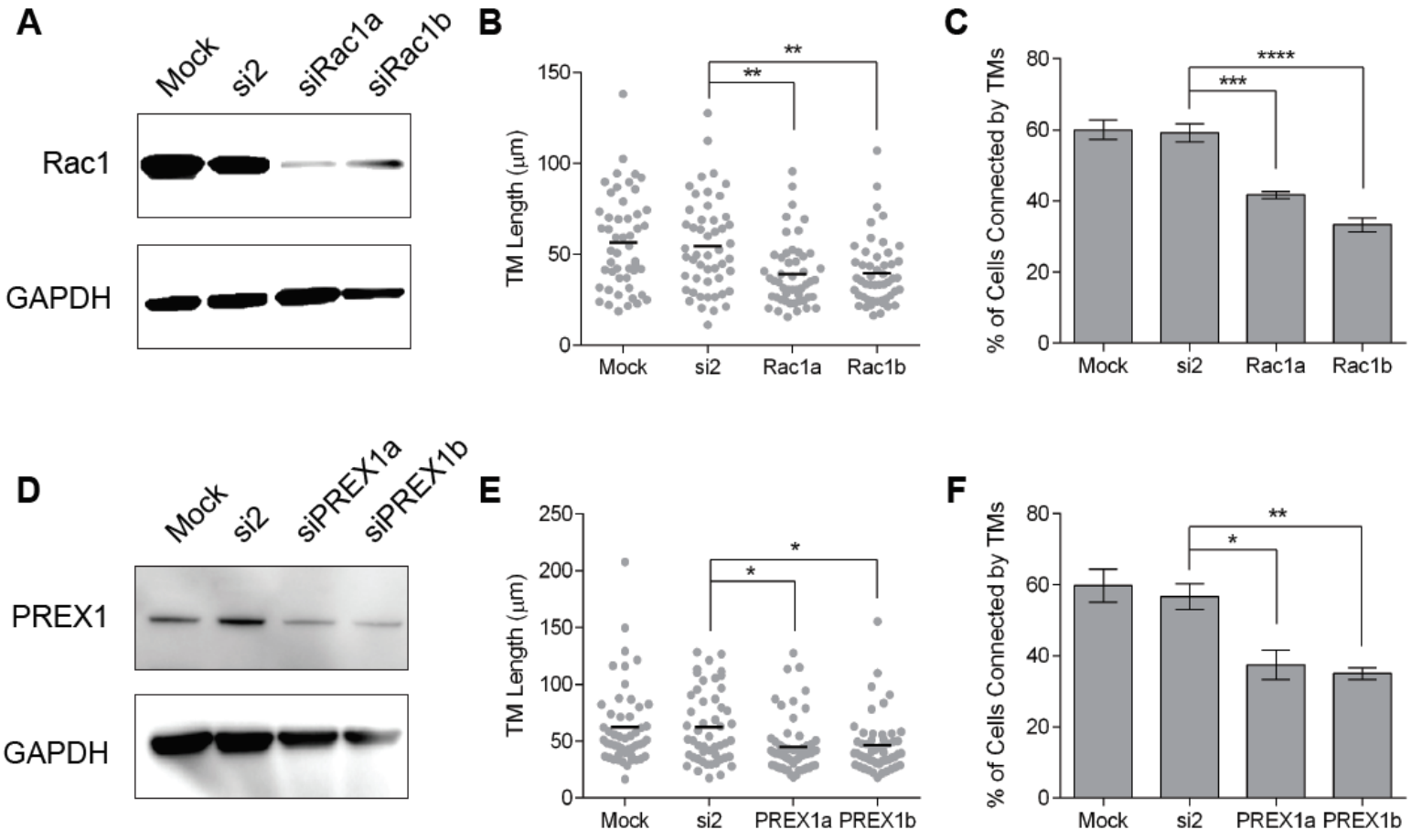
A
Mock
si2
siRac1a
siRac1b
Rac1
GAPDH
B
TM Length (μm)
150
100
50
0
**
**
Mock
si2
Rac1a
Rac1b
C
% of Cells Connected by TMs
80
60
40
20
0
****
***
Mock
si2
Rac1a
Rac1b
D
Mock
si2
siPREX1a
siPREX1b
PREX1
GAPDH
E
TM Length (μm)
250
200
150
100
50
0
*
*
Mock
si2
PREX1a
PREX1b
F
% of Cells Connected by TMs
80
60
40
20
0
**
*
Mock
si2
PREX1a
PREX1b

Figure 9. Knockdown of Rac1 and PREX1 impairs TM formation.

A & D. Western blots showing knockdown of Rac1 and PREX1 in PriGO8A cells, respectively, using two different siRNA duplexes for each protein, compared to cells receiving only oligofectamine (mock) or cells transfected with a non-targeting si2 control. **B-C.** Knockdown of Rac1 reduces the average TM length and the percent of cells connected by TMs (n = 50 TMs measured per siRNA duplex). **E-F.** Knockdown of PREX1 similarly impairs TM formation by reducing the average TM length and percent of cells connected by TMs *in vitro* (n ≥ 50 TMs measured per siRNA duplex).

- Add fields of view

4.7. Aim 7: Establish a *PREX1*-KO PriGO8A cell line using CRISPR/Cas9

To generate a *PREX1*-KO PriGO8A cell line, CRISPR/Cas9 was used. This technique is shown diagrammatically in Figure 10A. Clustered regularly interspaced short palindrome repeats (CRISPR)-associated (Cas9) nuclease was first discovered in bacteria as a mechanism of adaptive immunity for clearing foreign genetic material (119). Since its discovery, this system has been co-opted for genome editing in many different cell types, mainly because of its rapid, efficient, and highly targeted capacity for introducing genome edits. The CRISPR/Cas9 system uses a CRISPR RNA (crRNA) which consists of a 20-nucleotide sequence complementary to the target region in the genome (119). A second requirement of this system is that the target region immediately precedes a 5'-XGG-3' site, termed the protospacer adjacent motif (PAM). The PAM is recognized by the Cas9 nuclease and is required for DNA binding (119). The third component of this system is the trans-activating crRNA (tracrRNA) which fuses with the crRNA to form a single-guide RNA (sgRNA) complex that facilitates genome editing (119). The final component in this system is the Cas9 nuclease, which is guided to the target genome location by binding of the sgRNA complex at its complementary site (119). Once bound, the Cas9 nuclease cleaves the DNA 3 bases upstream of the PAM site, between the 17^{th} and 18^{th} bases of the target sequence (120). For our purposes, this allows highly targeted and specific cleavage of the *PREX1* gene. Once this cleavage occurs, the most common pathway of DNA repair used by the cell is the non-homologous end-joining pathway (NHEJ) (121). While this system acts rapidly, it is highly error-prone and often introduces random insertions and deletions into the DNA strand before ligating the two strands back together. Often, these result in frameshift mutations or the formation of a premature stop codon, both of which can result in a genetic knockout and total loss of functional PREX1 protein (121).

To detect and validate the introduction of a mutation in the *PREX1* gene, a T7 Endonuclease I (T7EI) assay was performed. This assay is commonly used to validate CRISPR knockouts by utilizing T7EI's ability to cleave mismatched DNA strands. This enzyme is a stable homodimer derived from bacteriophage T7 and composed of two catalytic domains connected by a bridge (122). After PCR amplification of a sequence of known length surrounding the target site, a heteroduplex formation step produces pairs of wild-type and mutation-bearing strands, as shown in Figure 10B. The presence of a base pair mismatch results in a kink in the DNA. T7EI resolves mismatched DNA strands by binding to the site of the mismatched DNA and introducing one nick on each strand. This occurs within 6 bases 5' of the mismatched site (123). This results in two differently-sized strands. The presence of two bands of different length, an indication of a mutation being successfully introduced at the target site, can be visualized by gel electrophoresis.

A

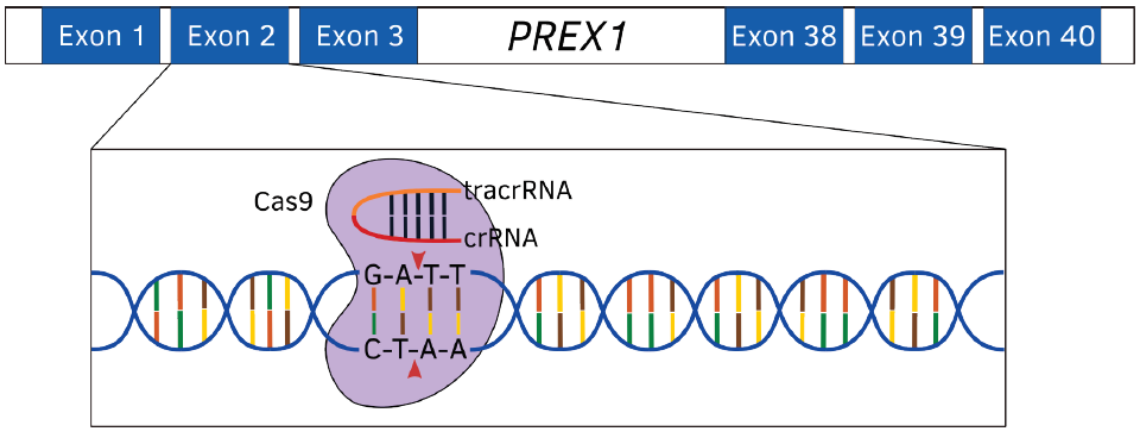
Exon 1
Exon 2
Exon 3
PREX1
Exon 38
Exon 39
Exon 40
Cas9
tracrRNA
crRNA
G-A-T-T
C-T-A-A

B


T7EI
PCR-Amplified
Target Region
200bp fragment
300bp fragment
CTL MX
Gel Electrophoresis

Figure 10. Graphical representation of CRISPR/Cas9 targeting the *PREX1* gene and the T7 Endonuclease I (T7EI) assay.

A. Depiction of the Cas9 enzyme and a guide RNA (gRNA) composed of a trans-activating CRISPR RNA (tracrRNA) and a CRISPR RNA (crRNA) targeting a 20-base pair sequence of exon 2 in the *PREX1* gene.

B. Depiction of the T7EI assay and a positive result indicating successful introduction of a mutation at the intended target site of the *PREX1* gene.

4.7.1. Lentiviral transduction

Lentiviral transduction was assessed first as a potential method of introducing CRISPR/Cas9 components into PriGO8A cells. Cells were first transduced with a *GFP*-containing lentivirus encoding a puromycin selection cassette. After selection, constitutive GFP expression was observed in all PriGO8A cells. Cells were then transduced with a lentiCRISPR GFP virus, encoding the Cas9 nuclease enzyme and a guide RNA targeting the *GFP* gene. After 48 hours, cells were imaged to quantify their expression of GFP. Compared to a non-transduced population of GFP-expressing cells, GFP was undetectable in approximately 30% of lentiCRISPR-transduced cells (Figure 11A-C). Furthermore, after several days of sustained Cas9 expression, PriGO8A cells eventually died in culture. This, combined with the incomplete knockout of GFP, suggested that alternative methods of CRISPR/Cas9 delivery should be explored.

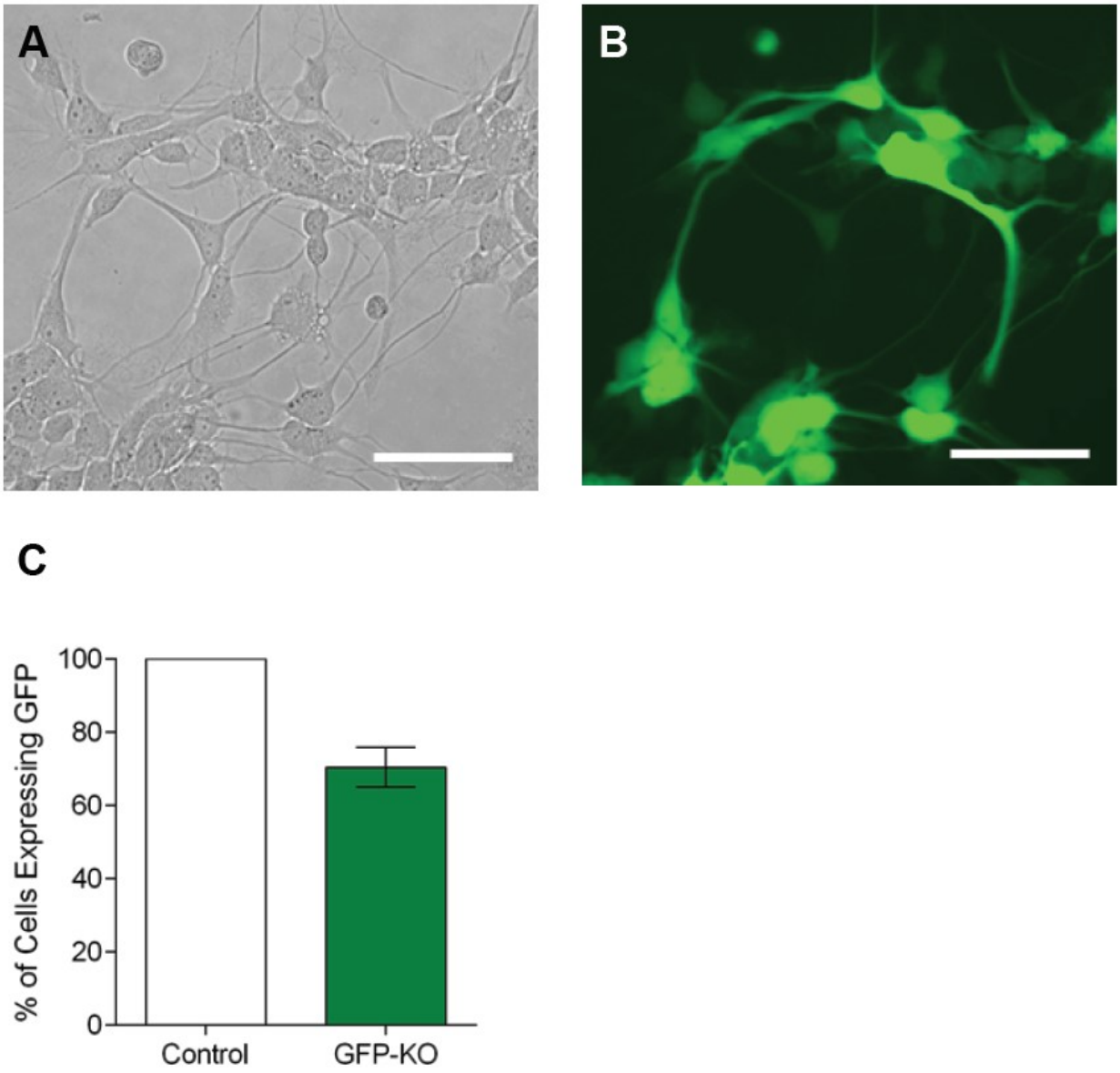
A
B
C
% of Cells Expressing GFP
100
80
60
40
20
0
Control
GFP-KO

Figure 11. LentiCRISPR virus targeting GFP reduces GFP expression in PriGO8A cells.

A-B. Representative images of reduced GFP expression in GFP-expressing PriGO8A cells transduced with a lentiCRISPR virus targeting GFP. Previously, selection by puromycin was performed to ensure all cells in the population expressed GFP. Scale bars = 100μm. **C.** Quantification of GFP-knockout PriGO8A cells compared to a control population of GFP-expressing PriGO8A cells demonstrates a reduction of approximately 30% in population-wide GFP expression.

4.7.2. Transfection

Subsequently, transfection was tested as a potential delivery method for CRISPR/Cas9 components. Transfection by lipofectamine has been performed in a number of studies to introduce CRISPR guide RNAs and Cas9 nucleases into cells *in vitro*, thus making it a potential agent for use in PriGO8A cells. Cells were transfected with purified Cas9 nuclease enzyme, a tracrRNA, and crRNA targeting exon 5 or exon 12 of the *PREX1* gene for 48 hours. These ready-made crRNAs were purchased from Dharmacon and specifically targeted *PREX1*. To optimize transfection for PriGO8A cells, a number of parameters were varied, including the duration of transfection, concentration of lipofectamine, and concentration of crRNA, tracrRNA, and Cas9 components. The final conditions tested were 5µl of lipofectamine, 25nM crRNA and tracrRNA, 10nM Cas9 nuclease, and 48 hours of incubation. A representative example of a T7EI assay after transfection under these conditions is shown in Figure 12. Despite repeated attempts to optimize transfection-mediated delivery of CRISPR/Cas9 reagents, no evidence of a mutation could be detected after amplification of the *PREX1* target sequence.

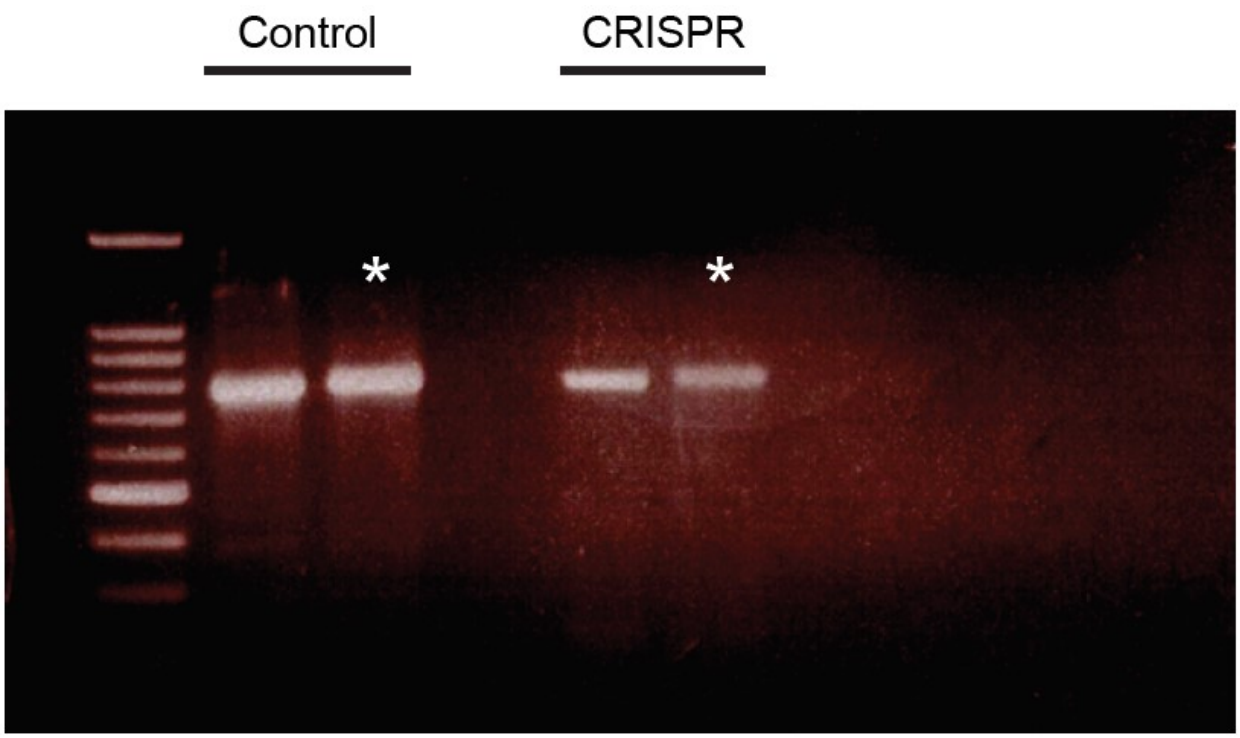
Control
CRISPR
*
*

Figure 12. Lipofection is not an efficient method for introducing CRISPR/Cas9 components into PriGO8A cells.

* indicates T7 endonuclease I (T7EI) enzyme incubation. PriGO8A cells were electroporated with purified Cas9, a fluorophore-conjugated tracrRNA, and a crRNA targeting exon 5 of *PREX1*. The predicted full-length parent band was 745bp, and the predicted digested band lengths were approximately 500bp and 245bp. Subsequent T7EI digestion did not produce any bands shorter than the full-length parent band, as shown, indicating that lipofection is not an effective means of introducing CRISPR components into PriGO8A cells.

4.7.3. Electroporation

Electroporation was then tested as a potential method of introducing a DNA plasmid encoding mCherry into PriGO8A cells. This was done with the goal of determining if cells could survive the electroporation process and express an inserted DNA plasmid. PriGO8A cells were electroporated with a mCherry-containing DNA plasmid using parameters from Thermofisher (A: rat astrocyte cell protocol, 1300V, 20ms, 2 pulses; B: U87MG cell protocol, 1300V, 30ms, 1 pulse) or the lab of Dr. William Stanford (C: 1050V, 30ms, 2 pulses) (Figure 13A). Three days later, flow cytometry was used to obtain the percentage of mCherry-positive cells. Protocol C was selected for downstream experiments because cells were able to survive and maintain robust expression of mCherry for several days after electroporation.

Electroporation of CRISPR/Cas9 components was then tested using a purified Cas9 enzyme, a fluorophore-conjugated tracrRNA, and three crRNAs targeting different exonic sequences in *PREX1:* target sequence #1: GCTAGAATGGAGGCGCCCAG, PAM: CGG, location: chr20: 48827844-48827866, exon 1; target sequence #2: CGGTGCCCAAGATCTCGTTG, PAM: AGG, location: chr20: 48827680-48827702, exon 1; target sequence #3: CGTTCTGCCGGATGCGATGC, PAM: AGG, location: chr20: 48747853-48747875, exon 2. These three crRNAs were custom-made and tested because they targeted early regions of the *PREX1* sequence, thus were more likely to introduce indel mutations into its functional domains. Introduction of the fluorophore-conjugated tracrRNA allowed visualization of cells that were successfully electroporated (Figure 13B). From the three crRNAs tested, the highest mutational efficiency was introduced with crRNA #3 targeting exon 2 (Figure 14; data not shown for other crRNAs). It was later discovered that the exon 1 sequences being targeted had high GC content,

which is known to increase the difficulty of on-target Cas9 cleavage activity as well as PCR amplification when detecting mutations.

To increase the mutational efficiency, a second round of electroporation targeting the same *PREX1* sequence was performed. Subsequently, limiting dilutions were performed in 96-well plates to expand single cells into clonal populations, with the intention of using populations with a complete *PREX1* knockout for downstream experiments. However, this proved to be unsuccessful because culture plates became contaminated on multiple occasions before the populations could grow sufficiently large to passage. Instead, dilutions were performed to give initial populations of approximately 200 cells so that they expanded faster and reduced the risk of contamination before passaging could be done. Seven populations grew sufficiently large to be passaged and T7EI screens were conducted on each population to identify those with the highest proportion of *PREX1*-KO cells for subsequent analysis (Figure 15A). The population that was chosen for further experimentation is indicated with a ▲, and was selected because it seemed to be enriched for *PREX1* mutations based on the intensity of fragments produced by the T7EI assay. Immunofluorescence for PREX1 was performed on the selected population and revealed that the majority of cells, 87%, had undetectable protein levels (Figure 15B). This was further validated with the online tool TIDE (Tracking of Indels by DEcomposition) which assesses the efficiency of genome editing at a target locus. This tool uses the quantitative trace data from Sanger sequencing reactions of control and mutated cells and then quantifies the efficiency of editing and characterizes the most common types of insertions and deletions. TIDE analysis identified 87.1% of genomic DNA containing indels that ranged from -10 to +2 bases in length (Supplementary Figure 5). Thus, although this represents a mixed population of PriGO8A cells, the presence of

site-directed mutations coupled with low levels of *PREX1* expression was deemed sufficient to assess the effects of *PREX1* deletion on PriGO8A TMs.

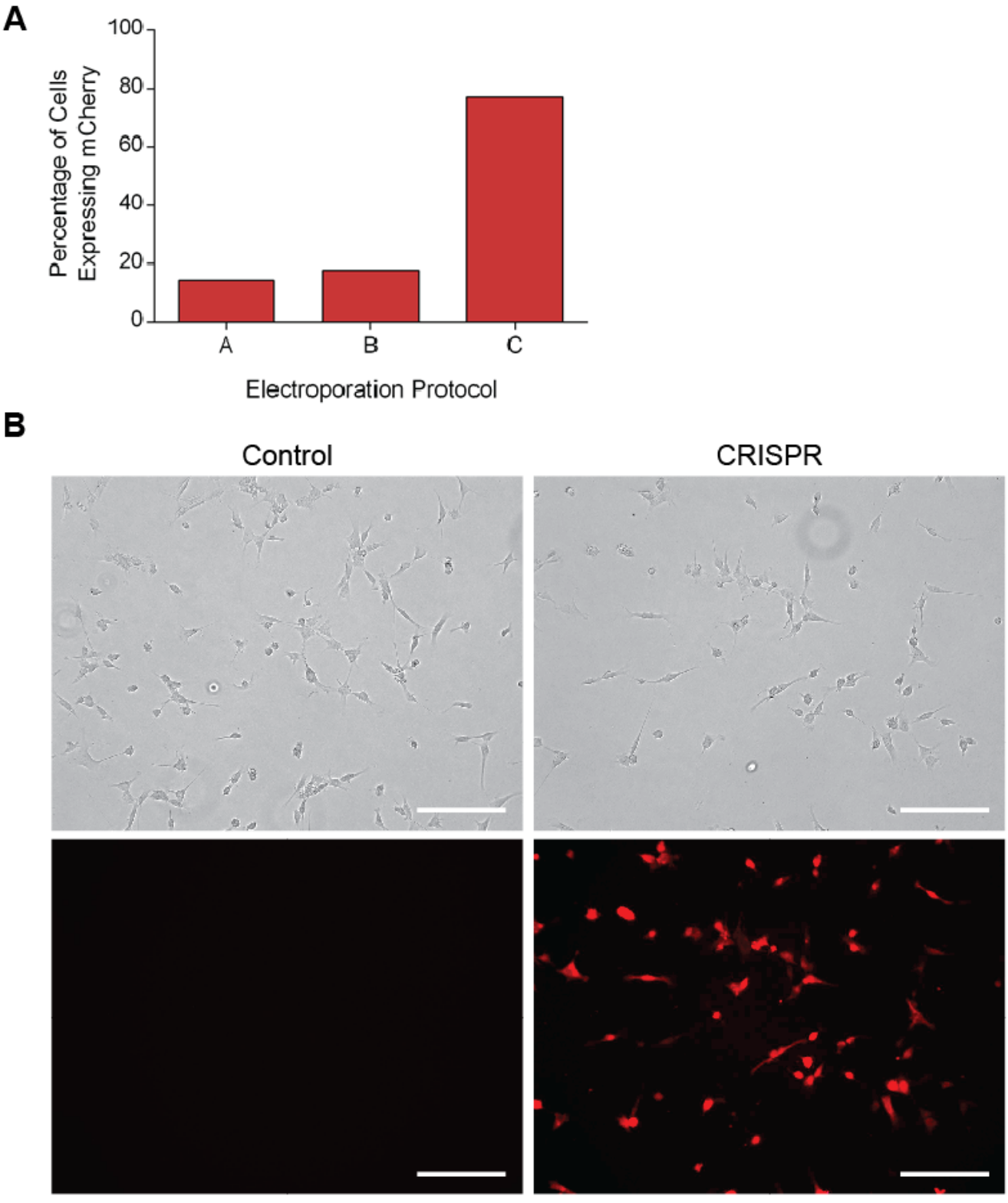
A
100
80
60
40
20
0
Percentage of Cells Expressing mCherry
A
B
C
Electroporation Protocol
B
Control
CRISPR

Figure 13. Electroporated PriGO8A cells can be visualized with a fluorophore-conjugated tracrRNA.

A. Flow cytometry results of PriGO8A cells electroporated with a mCherry-containing DNA plasmid using parameters from Thermofisher (A&B) or the Dr. William Stanford lab (C). Flow cytometry was performed three days later to quantify the percent of mCherry-expressing cells. **B.** Representative images of PriGO8A cells electroporated with CRISPR components according to protocol C. A fluorophore-conjugated tracrRNA (red) allows visualization of cells that were successfully electroporated. Scale bars = 200μm.

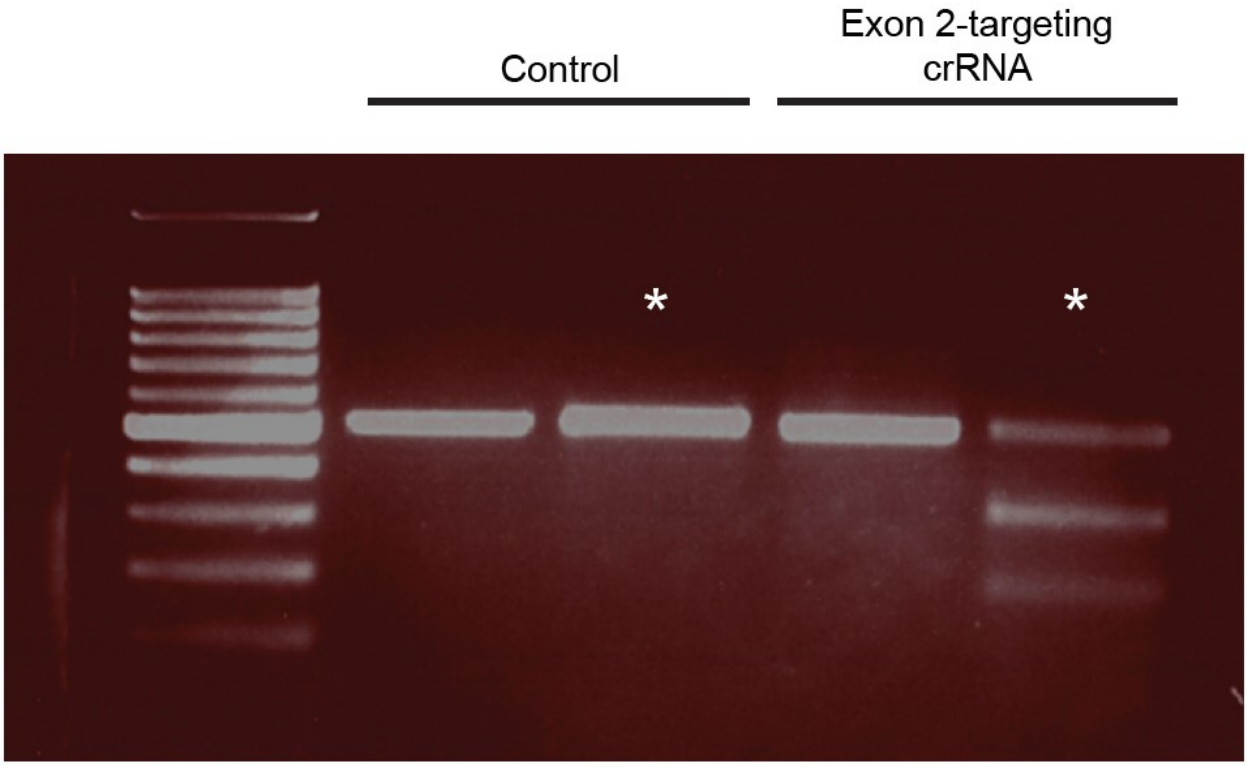
Control
Exon 2-targeting crRNA
*
*

Figure 14. A T7EI assay identifies *PREX1* mutations in electroporated PriGO8A cells.

PriGO8A cells were electroporated with Cas9 nuclease and either no gRNA or gRNA targeting exon 2 of *PREX1*. Three days after electroporation, cells were collected and the gRNA-targeted region was PCR-amplified. The predicted amplicon length is 515 nucleotides. * indicates PCR and subsequent T7EI digestion for 30 minutes. Successful heteroduplex digestion was predicted to result in fragment lengths of approximately 200 and 300 bases.

A

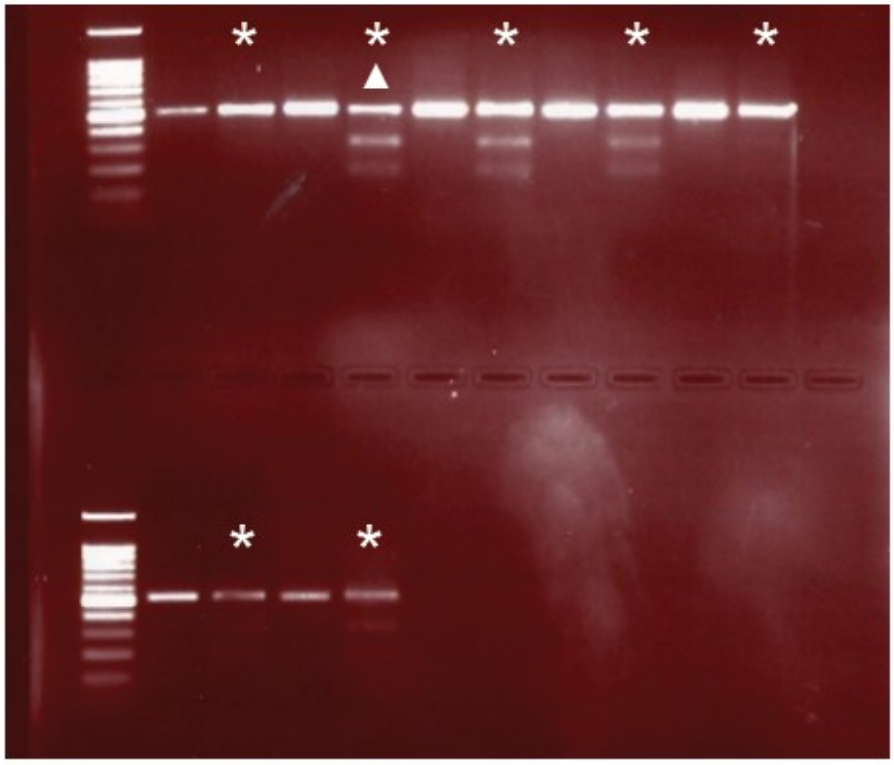

B

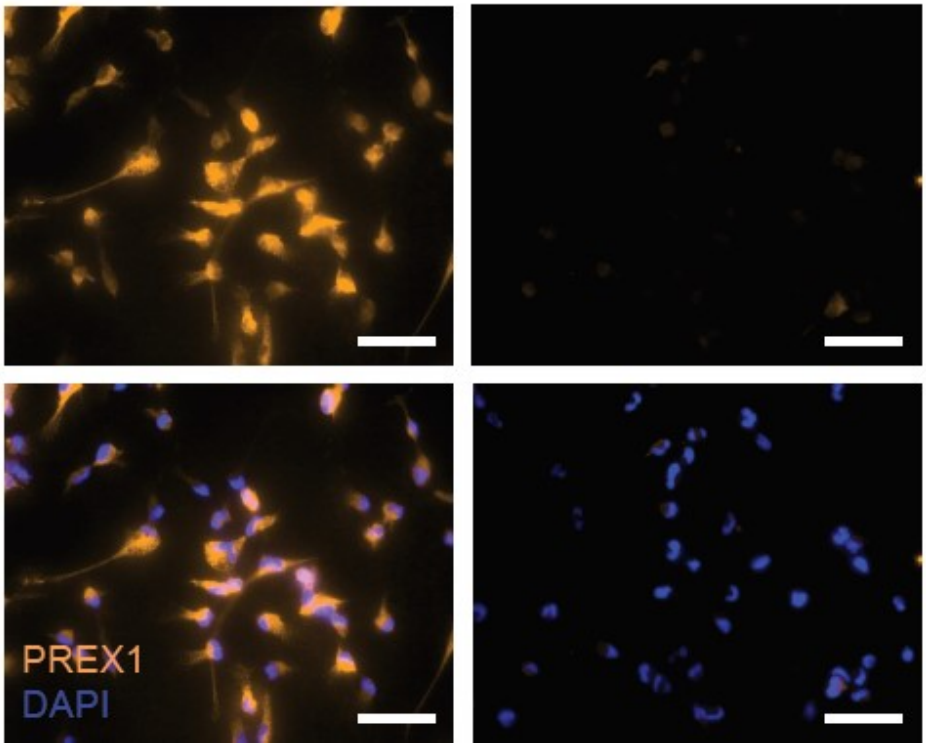

Figure 15. A T7EI assay can be used to screen for PREX1 mutations in polyclonal PriGO8A cell populations.

A. PriGO8A cells underwent a second round of electroporation with the same gRNA targeting exon 2 of *PREX1*. Cells were then grown in 96-well plates from starting populations of 200 cells. After expanding and passaging cells, T7EI assays (indicated by a *) identified polyclonal populations that were enriched for mutations in the targeted site of *PREX1*. **B.** Immunofluorescence for PREX1 revealed decreased protein expression in the population indicated by a ▲. Scale bar = 50μm.

4.8. Aim 8: Characterize the effect of *PREX1*-KO on PriGO8A TM formation

4.8.1. Cell motility, and TM length and connectivity

Videomicroscopy revealed a 46% reduction in motility of the modified population compared to wild-type PriGO8A cells (7.94µm per frame and 14.65µm per frame, respectively), which agrees with the effect seen in the PREX1 knockdown presented earlier and in previous reports of reduced PREX1 expression (32). Compared to control cells, *PREX1*-KO PriGO8A cells exhibited a significant reduction in TM length, with mean lengths of 62.67µm and 33.46µm, respectively. The percent of cells connected by TMs was also significantly reduced, with 58.25% of control cells and 31.67% of *PREX1*-KO cells connected. Altogether, these results provide further evidence for the role of PREX1 in TM biogenesis, as loss of PREX1 drastically impaired formation (Figure 16B-C).

4.8.2. Rescuing PREX1-*KO cells*

CRISPR/Cas9 was initially performed on PriGO8A cells at low passage, and *PREX1*-KO cells were subsequently carried for an extended period of time, possibly leading to genomic and phenotypic changes associated with high passage number. To determine whether this could be responsible for our findings, we transduced cells with a lentivirus housing the functional DHPH domain of *PREX1* under the control of a doxycycline-inducible promoter. *PREX1*-KO cells were cultured either in the absence or presence of doxycycline for 48 hours and assessed for their motility, TM length, and connectivity. Treating cells with doxycycline lead to a functional rescue of motility in the modified population when compared to untreated cells (13.53µm per frame and 8.07µm per frame, respectively; Figure 16D). Similarly, DHPH activity lead to an increase in TM length, with means of 36.72µm and 54.72µm in the untreated and doxycycline-treated *PREX1*-KO populations, respectively. The percent of cells connected by TMs also returned to baseline levels

after DHPH expression, as evidenced by TMs connecting 37.33% and 61.67% of cells in the untreated and treated populations, respectively (Figure 16E-F). Altogether, this suggests that our findings in *PREX1*-KO cells are indeed due to the loss of PREX1 signaling and can be rescued by re-introducing the protein's functional DHPH domain.

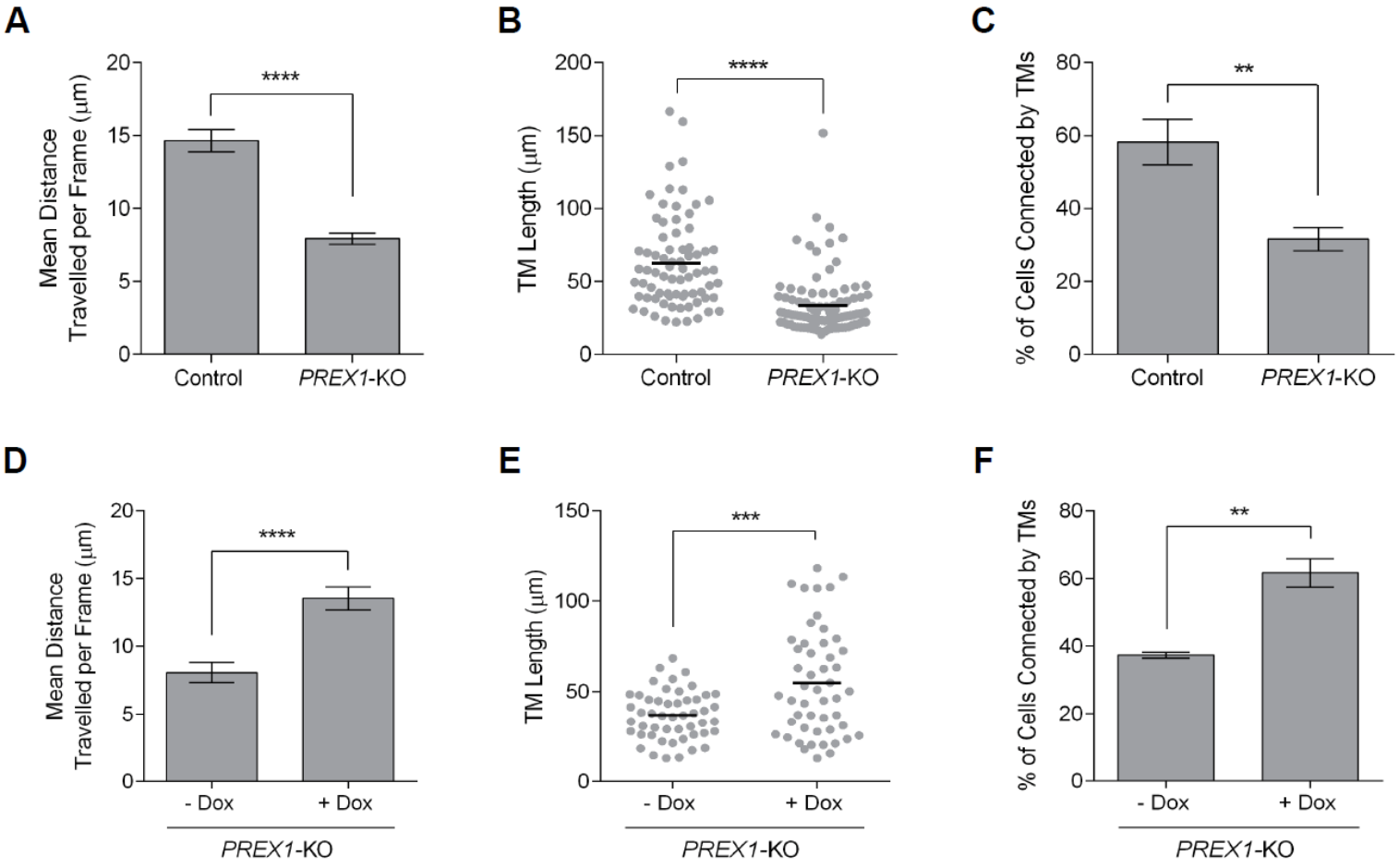
A
Mean Distance Travelled per Frame (μm)
20
15
10
5
0
****
Control
PREX1-KO
B
TM Length (μm)
200
150
100
50
0
****
Control
PREX1-KO
C
% of Cells Connected by TMs
80
60
40
20
0
**
Control
PREX1-KO
D
Mean Distance Travelled per Frame (μm)
20
15
10
5
0
****
- Dox
+ Dox
PREX1-KO
E
TM Length (μm)
150
100
50
0
***
- Dox
+ Dox
PREX1-KO
F
% of Cells Connected by TMs
80
60
40
20
0
**
- Dox
+ Dox
PREX1-KO

Figure 16. Knockout of *PREX1* impairs cell motility and TM formation and can be rescued by expression of the functional DHPH domain of *PREX1*.

A. *PREX1*-KO PriGO8A cells exhibit reduced motility compared to their wild-type counterparts when tracked by videomicroscopy. **B-C.** Knockout of *PREX1* impairs TM biogenesis by reducing the average TM length and the percent of PriGO8A cells connected by TMs. **D-F.** The functional impairment observed in *PREX1*-KO PriGO8A cells can be partially rescued by expression of the functional DHPH domain of *PREX1*.

5. Discussion

Despite the availability of surgical and adjuvant therapies for treating glioblastoma, the mortality rate of patients with this disease remains startlingly high (124). Recent characterization of TMs in an *in vivo* model of glioblastoma has shed light on a novel mechanism of treatment resistance and tumor dissemination that has not been previously described in this disease (71). The authors of this study were unable to demonstrate TM growth in primary glioblastoma cells cultured *in vitro* and grown as neurospheres, which is consistent with previous findings of neurosphere models (36). Presumably, because the cells were not grown on a laminin-coated surface, they were unable to form a monolayer and extend cellular protrusions that are the precursors to TMs. However, the conclusions of this study emphasize the need for further examination of glioblastoma TM biology so that future treatment approaches can target and disrupt the functional network connecting cells. Thus, there is a pressing need for a cell culture model of glioblastoma TMs that would allow rapid and manipulable structural and functional characterization of these structures.

5.1. PriGO TM structure and function

The study here presents the first instance of TMs being characterized in an *in vitro* model of patient-derived glioblastoma cells cultured as a monolayer. A key requirement for characterizing this model is culturing PriGO cells on laminin, thereby allowing the cells to adhere to a surface, form a monolayer, and extend cellular projections. For this study, the term ‘tumor microtube’ was chosen rather than ‘tunneling nanotube’ because it is consistent with Osswald *et al.*’s work which was the first to characterize cell-to-cell connections in a glioblastoma model. Before performing qualitative and quantitative assessments of tumor microtubes, a definition for the term was established to refer to structures that: 1) form a physical connection between two PriGO cells; 2)

are elevated from the surface *in vitro* and do not adhere to the culture plate; and 3) contain actin among their structural components. Though TMs have not been consistently referred to by a single definition in the literature, the definition chosen here represents many of the characteristics that are repeatedly described in studies of TNTs (53,55,60,68).

This presents a few challenges. Firstly, for the purposes of quantification, the most strictly adhered to aspect of the definition is the first criterion: TMs are structures that form physical connections between two PriGO cells. While this study reports a number of results that support the latter two criteria, it was not feasible to assess these characteristics in every structure that was measured. Thus, an assumption, and potential weakness, of this work is that any structure connecting two PriGO cells represents a TM. To verify the results presented here, ideally future studies would be able to take advantage of a TM-selective marker that would allow for the most accurate assessment of these structures *in vitro*. However, to date, no TM-specific protein marker has been identified, thus restricting this and other work to using morphological and functional qualities to report on these structures (54). Furthermore, while the majority of the existing literature also establishes the second criterion – forming above the substrate surface – as imperative to TM labelling, a follow-up study to the work reported by Osswald *et al.* referred to non-connecting extensions of primary glioblastoma cells as TMs (125). As the ADP formation mechanism demonstrates, TMs are capable of forming from a previously-unconnected cellular extension. However, TMs have also been reported to have structural properties and signaling pathways that diverge from other cellular extensions, such as filopodia and lamellipodia (refer to Table 1 on page 11). Thus, referring to the structures in the follow-up study as TMs may be a naive assumption to make since many filopodia-like protrusions are seen to form and retract *in vitro* without contacting other cells (57). Indeed, a priority for the field going forward should be to identify the proteins that

delineate TMs from non-connecting projections. The unique characteristics of TMs, such as their non-adherence to the substrate, strongly suggests that non-overlapping signaling pathways must be at play to orchestrate these properties.

The results presented here demonstrate that PriGO cells form TMs *in vitro* that meet the three criteria presented earlier: actin-containing structures that connect cells together and form above the substrate (Figure 1). Cells obtained from different patients with glioblastoma were all capable of forming TMs but exhibited heterogeneity with respect to their average length and the percent of cells connected by TMs (Figure 2). Compared to TMs formed *in vivo* which reached lengths of over 500µm, PriGO cells most often formed TMs in the range of 50-100µm, and infrequently extended these over 200µm. Furthermore, although different cell lines occupied a similar range of TM lengths, much larger differences were seen in the percent of cells connected by TMs. The greatest difference was observed between the PriGO7A and PriGO8A lines, which formed TMs between 36.22% and 68.12% of cells, respectively, suggesting that PriGO8A cells are capable of forming a much more interconnected network. This is in line with the *in vivo* phenotype of PriGO8A cells reported by Gont *et al.* (36). When injected intracerebrally into mice, PriGO8A cells formed an invasive tumor that extended into the uninjected hemisphere via the corpus callosum, thus recapitulating many of the features of GTICs described previously. Characterization of the percent of cells with ≥ 1 TM revealed that, although PriGO7A cells are the least connected, individual cells form 2 TMs much more often than cells of any other line, all of which predominantly form 1 TM per cell. Across all lines, cells that form 3 or more TMs were rarely seen.

Based on previous studies, it is unclear how TNT formation is induced. However, studies of T lymphocytes and NK cells have found that a longer duration of cell-cell contact before separation

increases the likelihood of TNT formation (126,127). The same study found that a greater degree of receptor/ligand interaction was also associated with a higher likelihood of forming TNTs, presumably because this led to a greater duration of cell-cell contact. Our findings are consistent with the results of previous studies elucidating the mechanisms by which TMs form; PriGO TMs are capable of forming using both the cell dislodgement mechanism and ADP mechanism but show preference for the former (Figure 3). *In vivo*, this would suggest that glioblastoma cells are more likely to be connected by short-distance local networks than by distant connections driven by searching protrusions. However, in this study, ADP-derived TMs were more likely to connect cells over larger distances and persist for a longer period of time than dislodgement-derived connections, thus they represent an important part of the cellular network. The longest-lived TMs remained in culture for over 3 hours. Although this represents the upper limit of lifetimes recorded *in vitro*, it is still significantly shorter than Osswald *et al.*'s observations which showed TMs surviving for up to several days. This difference may be due to factors *in vivo* that support and stabilize TMs for longer periods of time, thus it is worth considering whether *in vitro* conditions could be optimized to promote longer-term TM growth.

Conducting an analysis of TM lifetime and maximum length presented a technical challenge and limitation to the results reported here. Videomicroscopy recordings were performed using a 10X objective to capture many cells in the same frame while still allowing changes in cellular morphology to be detected. However, if TMs were already formed when the video started, or if they persisted beyond the end of the video, their lifetime was not recorded since the start/end time could not be determined. This restriction would affect long-lasting TMs more than transient TMs, thus potentially skewing the results of TM lifetime to seem shorter-lived. Furthermore, if a TM's length stretched beyond the objective's field of view, it was not recorded since the full length could

not be accurately measured. Again, this would mostly limit recordings of far-reaching TMs, potentially skewing the results towards shorter maximum lengths. These parameters were abided by to improve the accuracy of the reported measurements, and while they did not often restrict which TMs could be measured, it is a limitation worth noting in this study.

Structurally, PriGO cells contained a number of the proteins that were identified *in vivo* by Osswald *et al*. (Figure 4). TMs stained positively for actin, β-tubulin, and non-muscle myosin IIA. Future work would benefit from assessing the presence of endoplasmic reticulum and microvesicles, and the absence of myosin-X, in TMs to further confirm that their contents mirror those seen *in vivo* (74). Characterization of the PriGO TM-TM boundary by transmission electron microscopy revealed similarities with past reports of Cx43-containing gap junctions in hippocampal neurons and interneurons (128,129). Namely, past reports characterize gap junctions by increased protein densities at the site of contact between two cells, association for several hundred nanometers, and a nanometer-scale gap between cells (130). These observations were also seen in PriGO TMs imaged by transmission electron microscopy (Figure 5). To validate the presence of Cx43-containing gap junctions between cells, Cx43 immunofluorescence was also performed in PriGO8A cells (Figure 6). Staining of Cx43 does not mirror what is seen by performing immunohistochemistry on tissue sections (71). However, the pattern detected was consistent with previous reports of Cx43-positive staining in glioma cells, colorectal cancer cells, hippocampal neurons, and astrocytes (131–135). Thus, based on transmission electron micrographs depicting gap junction-like structures and a pattern of Cx43 staining that is consistent with previous reports, it is feasible to conclude that PriGO TMs connect cells by Cx43-containing gap junctions.

Osswald *et al.* describe multiple functions of TMs *in vivo*, including permitting directed travel of nuclei and mitochondria, propagating intercellular calcium waves, and mediating resistance to cytotoxic therapy (74). The authors also demonstrate that cargo exchange via TMs was restricted to calcium ions and did not permit mitochondrial or protein transfer. The latter phenomenon was also confirmed in PriGO TMs *in vitro* (Figure 7). After performing videomicroscopy on PriGO cells in culture for up to 24 hours, no exchange of mitochondria, GFP, or mCherry could be detected, providing further evidence that PriGO TMs recapitulate the structure of the TMs identified *in vivo* and may carry out similar functions. The next step is to evaluate whether TMs *in vitro* can be used to propagate intercellular calcium waves and facilitate electrical connectivity between cells.

5.2. PREX1 is a novel player in PriGO TM biogenesis

Interestingly, this study also casts light on PREX1 as a novel player in the formation and growth of glioblastoma TMs. Immunofluorescence positively stains for PREX1 and Rac1 throughout the length of TMs (Figure 8). Subsequent knockdown of both proteins impaired both TM length and TM connectivity, implicating both proteins in glioblastoma TM biogenesis for the first time (Figure 9). The significance of this finding is worth noting in particular because Rac1 has previously been shown to have a cell type-specific role in TNT biogenesis. For example, while inhibition of Rac1 has been shown to reduce TNT formation and growth in macrophages, the same experiments had no effect on TNTs connecting HeLa cells (55,68).

Subsequently, multiple methods of performing CRISPR/Cas9 were tested on PriGO8A cells to determine the best approach for introducing a knockout mutation into the *PREX1* gene.

Although lentiviral transduction and lipofection were ineffective at introducing mutations, electroporation successfully introduced CRISPR/Cas9 components into cells and inserted indel mutations into the target *PREX1* site (Figure 11-15). Knockout of *PREX1* could be detected by immunofluorescence and negatively labelled the majority of cells, with only a small number retaining low levels of *PREX1* expression. *PREX1*-KO cells were subsequently characterized for their motility, TM length, and TM connectivity compared to a control population of cells. A significant reduction in all three metrics was evident, thus implicating the loss of PREX1 signaling in the reduced ability of PriGO cells to form TMs to other cells and to extend these connections over long distances. Indeed, loss of *PREX1* is also not functionally redundant, as its activity could not be completely compensated for by other Rac-GEFs, such as TIAM1 and VAV1. However, because motility and TM growth were not abolished completely, this suggests that Rac1 was still active in coordinating downstream activators of cytoskeletal reorganization and motility. Thus, it is likely that other Rac-GEFs are maintaining a basal level of Rac1 activity.

These findings highlight PREX1 as a component in the cascade of events that initiate, and contribute to, the formation and growth of PriGO TMs. This is presented diagrammatically in Discussion Figure 1. However, the fact that some cells retained low levels of *PREX1* expression presents a challenge to interpreting these findings. While some cells stained negatively for PREX1, the results of motility and TM formation aggregate data from the population as a whole, so include cells that retained low levels of *PREX1* expression. Thus, it is possible that a more pronounced phenotype, with regards to both motility, TM biogenesis, and other aspects of cell growth, would have been observed if a population of complete *PREX1*-KO cells was characterized. Our lab recently established PriGO cell lines with complete loss of *PREX1* by isolating and expanding

clonal populations. This will allow validation of the results reported here, as well as additional characterization of how loss of PREX1 signaling affects PriGO cell growth and motility.

Importantly, the effect of *PREX1*-KO in this study could be functionally rescued by reintroducing a truncated constitutively active version of *PREX1* by lentiviral transduction (Figure 16). As described previously, high passage number can substantially alter cellular morphology, gene expression, response to stimuli, and growth rates compared to early passage cells–an effect which has been documented in glioma cultures previously (136,137). Thus, the ability to observe a restoration of cellular motility and TM growth provides evidence that the loss of *PREX1* expression is likely responsible for the impairment in cell motility and TM formation, rather than the continued passage of cells.

5.3. Towards development of a TM-targeting therapeutic strategy

Future studies would benefit greatly from determining whether PriGO cells are capable of using TMs to facilitate calcium ion transfer and whether a model of TM-dependent treatment resistance can be devised to advance development of targeted therapeutic approaches. As previously mentioned, Osswald *et al.* speculated that *in vivo* TMs are critical mediators of calcium homeostasis that are required for network integration (71). The authors showed that the increases in intracellular calcium levels that occur with radiotherapy-induced cytotoxicity can be mitigated by enhanced cellular connectivity. Connected glioblastoma cells could distribute calcium throughout their TM network to reach non-lethal levels, which their non-connected counterparts were unable to do. Indeed, *Cx43* expression in glioblastoma cells has been shown previously to be a mediator of TMZ resistance (132,138–140). Overexpression of *Cx43* in glioblastoma cell lines

was sufficient to render cells resistant to TMZ treatment, while siRNA- or antibody-mediated reductions in Cx43 levels led to the opposite phenomenon and restored TMZ sensitivity (132,139,140). Cx43-mediated resistance has been reported to occur via gap junction-dependent and gap junction-independent pathways (132,141). One mechanism that contributes to this involves Cx43-mediated activation of the AKT/AMPK/mTOR pathway which upregulates pro-survival gene expression and blocks cell death. Blocking this pathway was shown to synergize with Cx43 inhibition to induce autophagy and cell death (141). Other studies have shown Cx43 to be inversely related to *Bax* and *Bcl-2* expression and Cytochrome C release, suggesting that Cx43 is linked to the mitochondrial apoptosis pathway (132). Thus, it seems that the ability of glioblastoma cells to propagate calcium waves is essential to achieving radioresistance in a network-dependent manner.

Designing targeted therapeutic strategies for glioblastoma requires a thorough understanding of the signaling pathways underlying its invasive behavior. The recent discovery of TMs in glioblastoma suggests that dismantling the cancer's intratumoral network could contribute to prolonged patient survival and better outcomes. Indeed, Osswald *et al.*'s *in vivo* report has already demonstrated that the heightened resistance to radiotherapy amongst functionally interconnected cells can be rapidly undermined by blocking connectivity via knockdown of GAP-43 (71). Thus, these findings demonstrated that glioblastoma tumors frequently form TMs that are important for their overall growth. Osswald *et al.* also performed a structural investigation of oligodendrogliomas–tumors with 1p/19q codeletion–and found that these tumors infrequently form TMs. Clinically, patients with oligodendroglioma demonstrate a high responsiveness to combined radio- and chemotherapy and high levels of tumor apoptosis; analyses of two phase III studies showed long-term survival in 40-50% of patients receiving this treatment regime

(16,142,143). While glioblastoma and oligodendroglioma likely have differing cells of origin with different genetic and molecular profiles, these findings also suggest that 1p/19q chromosomal loss may contribute to this difference in phenotype (71). Thus, the link between TM growth and 1p/19q codeletion would be interesting to explore further.

5.4. Conclusion

Glioblastoma is a heterogeneous brain tumor with limited treatment options for afflicted individuals. Several barriers exist to reducing glioblastoma's high mortality rate, including the high rate of recurrence and treatment-resistant nature of the disease. Developing targeted therapies must begin with a comprehensive understanding of glioblastoma's underlying biology, and great strides have been taken in the past several decades to dissect the genetic and molecular drivers of this disease. The recent discovery of functionally interconnecting TMs in an *in vivo* model of glioblastoma is one such contribution. These structures were GAP43-dependent and mediated treatment resistance largely by reducing intracellular calcium levels. The authors posited that other signaling molecules, such as ATP, miRNAs, IP3, are also gap junction-permeable molecules that could potentially be transferred via TMs, but this has yet to be confirmed. Ultimately, further exploration of the functions of glioblastoma TMs will be a necessary step in the development of new and targeted treatment options.

Here, we present the first characterization of an *in vitro* model of TMs in patient-derived glioblastoma cells. Demonstrating that these structures recapitulate many of the structural and functional characteristics of *in vivo* TMs was a vital first step in ensuring that this is an accurate model on which to base future studies. Our characterization of *PREX1* knockdown and knockout PriGO cells has also added another piece to our understanding of TM formation. With this model

of glioblastoma TMs, future studies are primed to untangle the complex network that orchestrates TM growth and function.

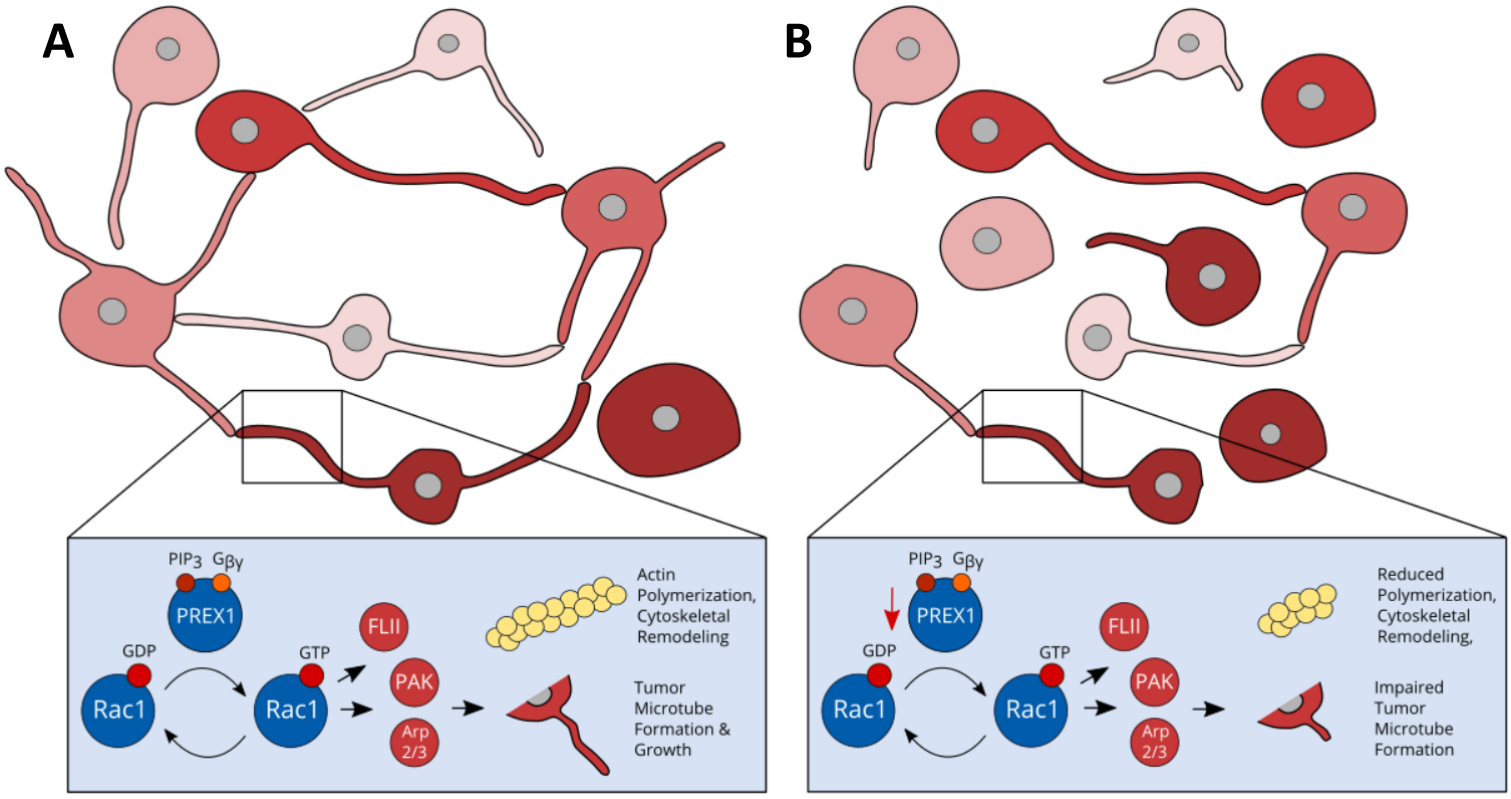
A
PIP3 Gβγ
PREX1
GDP
GTP
Rac1
Rac1
FLII
PAK
Arp 2/3
Actin Polymerization, Cytoskeletal Remodeling
Tumor Microtube Formation & Growth
B
PIP3 Gβγ
PREX1
GDP
GTP
Rac1
Rac1
FLII
PAK
Arp 2/3
Reduced Polymerization, Cytoskeletal Remodeling,
Impaired Tumor Microtube Formation

Discussion Figure 1. Model depicting knockout of PREX1 and the resulting effect on TM formation and growth.

A. Under normal conditions, PriGO8A cells form TMs *in vitro* which requires signaling through Rac1 and its GEF, PREX1. Activation of downstream effectors promotes cytoskeletal reorganization and actin polymerization leading to the formation and growth of TMs. **B.** In *PREX1*-KO PriGO8A cells, Rac1 frequently remains GDP-bound and, therefore, is unable to activate downstream signaling pathways that lead to TM growth. As a result, cells form TMs less frequently and, when they do, form shorter connections.

6. Appendix

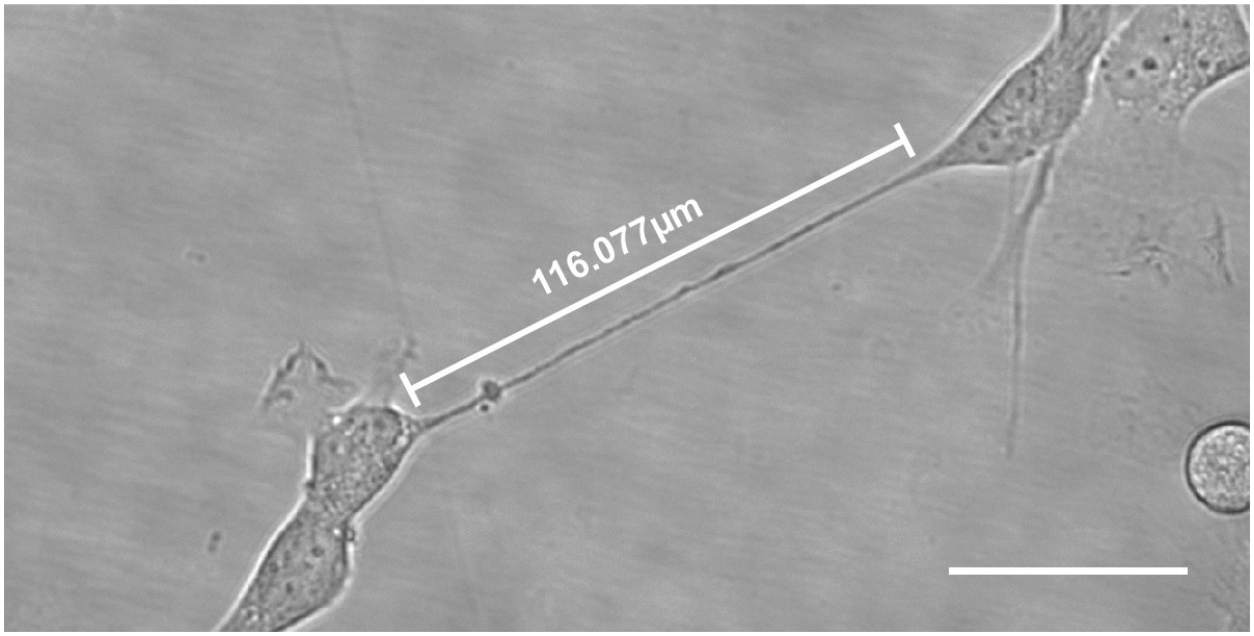

Supplementary Figure 1. Example of TM length quantification.

Example of two PriGO8A cells sharing a TM connection *in vitro.* TMs were measured from the narrowest point of one cell preceding the TM to the narrowest point of the connected cell before the cell body. Measurements were recorded in µm. Scale bar = 50µm.

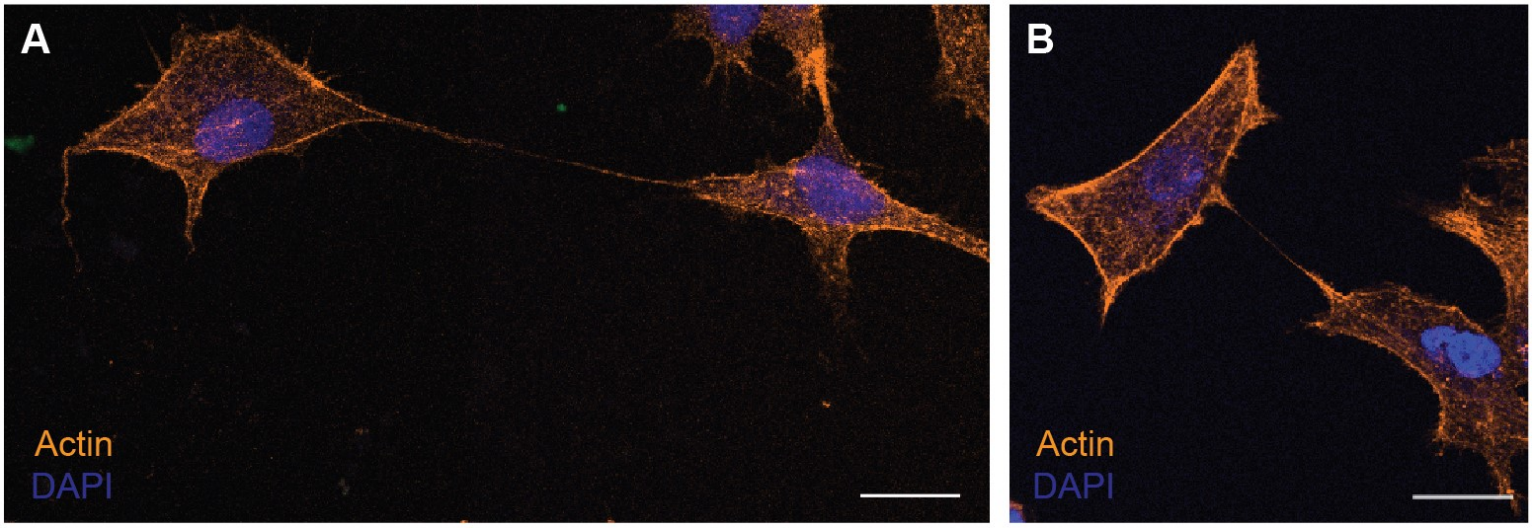
A
Actin
DAPI
B
Actin
DAPI

Supplementary Figure 2. PriGO9A and PriGO17A cells stain positively for actin filaments. **A-B.** Actin staining in PriGO9A and PriGO17A cells, respectively. Actin is found within the length of PriGO TMs *in vitro*. 63X images were acquired by confocal microscopy. Scale bars = 20μm.

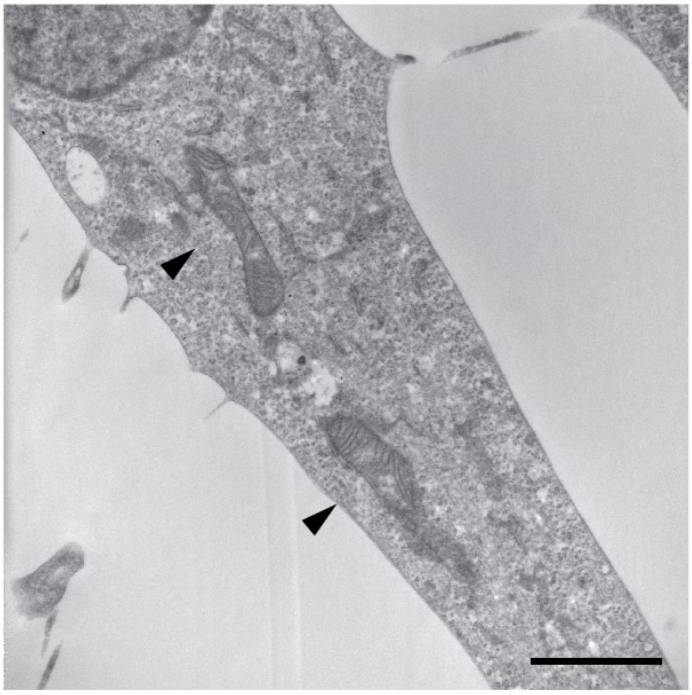

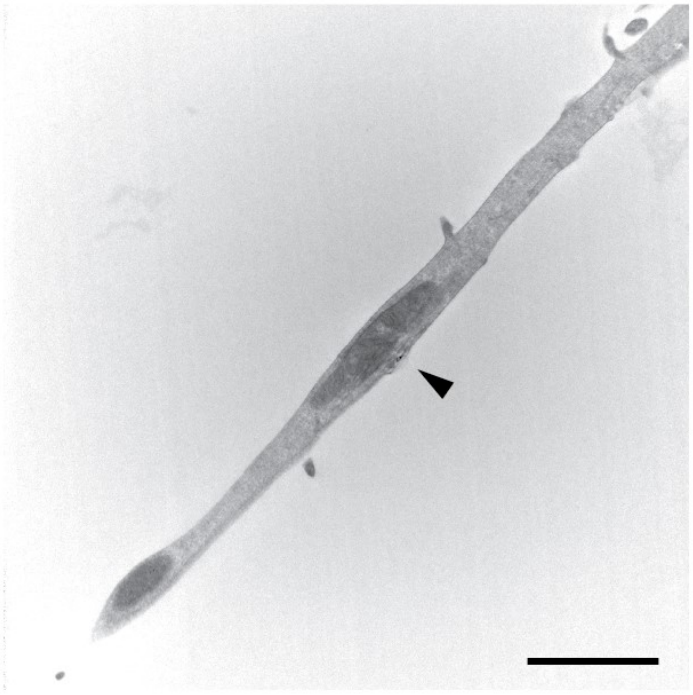

Supplementary Figure 3. TEM micrographs of mitochondria in PriGO8A cell projections.

Mitochondria can be detected within the length of PriGO8A cell projections by transmission electron microscopy (indicated by ►).

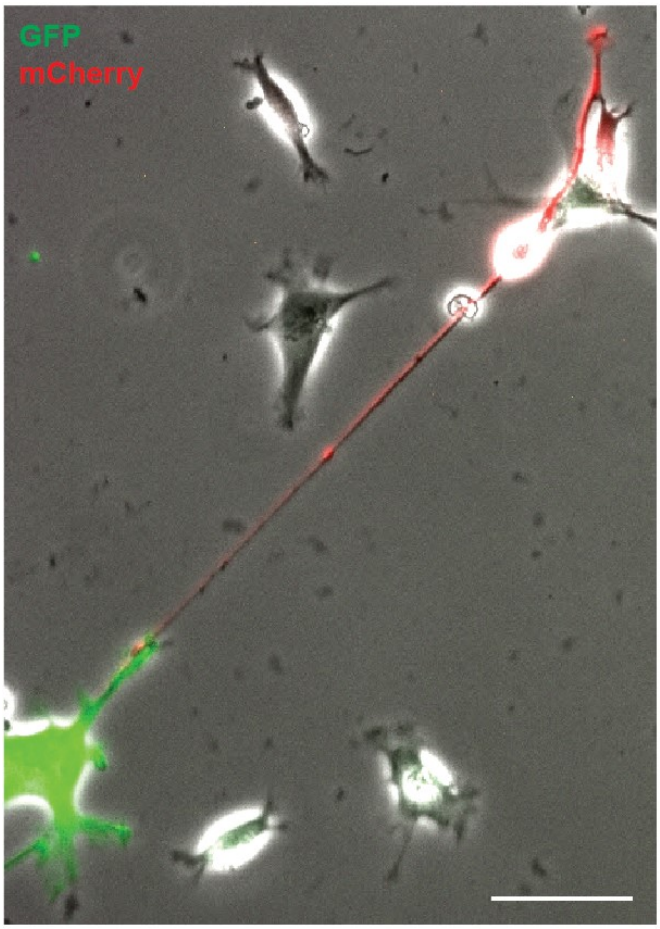
GFP
mCherry

Supplementary Figure 4. Videomicroscopy of GFP- and mCherry-expressing PriGO8A cells connected by a TM.

GFP- and mCherry-expressing PriGO8A cells are connected by a TM formed via the ADP mechanism. Fluorescent protein expression shows the point of contact between both cells. This is evidence for two protrusions from separate cells forming a physical contact and connecting the cells together.

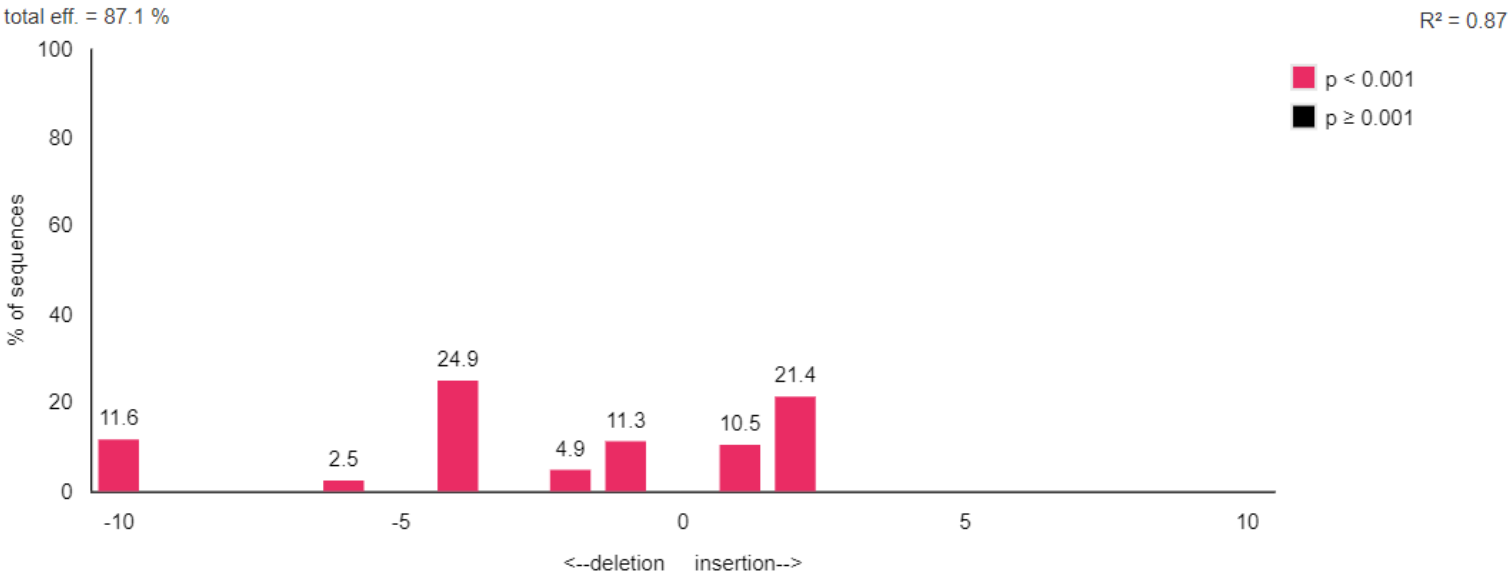
total eff. = 87.1 %
R² = 0.87
p < 0.001
p ≥ 0.001
% of sequences
100
80
60
40
20
0
11.6
2.5
24.9
4.9
11.3
10.5
21.4
-10
-5
0
5
10
<--deletion
insertion-->

Supplementary Figure 5. TIDE analysis characterizes the type of *PREX1* mutations in PriGO8A cells.

A-B. TIDE analysis of *PREX1*-KO PriGO8A cells identifies a total mutational efficiency of 87.1% and a distribution of indel mutations in the target sequence of exon 2. Indels of varying sizes were detected within the range of -10 to +2 base pairs. The high mutational efficiency corroborates the lack of PREX1 protein observed upon immunofluorescence staining.

7. References

1. Omuro A. Glioblastoma and Other Malignant Gliomas: A Clinical Review. JAMA. 2013 Nov 6;310(17):1842.

2. Louis DN, Perry A, Reifenberger G, von Deimling A, Figarella-Branger D, Cavenee WK, et al. The 2016 World Health Organization Classification of Tumors of the Central Nervous System: a summary. Acta Neuropathologica. 2016 Jun;131(6):803–20.

3. Dolecek TA, Propp JM, Stroup NE, Kruchko C. CBTRUS Statistical Report: Primary Brain and Central Nervous System Tumors Diagnosed in the United States in 2005-2009. Neuro-Oncology. 2012 Nov 1;14(suppl 5):v1–49.

4. Yuile P, Dent O, Cook R, Biggs M, Little N. Survival of glioblastoma patients related to presenting symptoms, brain site and treatment variables. Journal of Clinical Neuroscience. 2006 Aug;13(7):747–51.

5. Cuddapah VA, Robel S, Watkins S, Sontheimer H. A neurocentric perspective on glioma invasion. Nature Reviews Neuroscience. 2014 Jul;15(7):455–65.

6. Clavreul A, Guette C, Faguer R, Tétaud C, Boissard A, Lemaire L, et al. Glioblastoma-associated stromal cells (GASCs) from histologically normal surgical margins have a myofibroblast phenotype and angiogenic properties: GASCs in glioblastoma surgical margins. The Journal of Pathology. 2014 May;233(1):74–88.

7. Montana V, Sontheimer H. Bradykinin Promotes the Chemotactic Invasion of Primary Brain Tumors. Journal of Neuroscience. 2011 Mar 30;31(13):4858–67.

8. Hou LC, Veeravagu A, Hsu AR, Tse VCK. Recurrent glioblastoma multiforme: a review of natural history and management options. Neurosurgical Focus. 2006 Apr;20(4):E3.

9. Agnihotri S, Burrell KE, Wolf A, Jalali S, Hawkins C, Rutka JT, et al. Glioblastoma, a Brief Review of History, Molecular Genetics, Animal Models and Novel Therapeutic Strategies. Archivum Immunologiae et Therapiae Experimentalis. 2013 Feb;61(1):25–41.

10. O'Reilly SM, Newlands ES, Brampton M, Glaser MG, Rice-Edwards JM, Illingworth RD, et al. Temozolomide: a new oral cytotoxic chemotherapeutic agent with promising activity against primary brain tumours. European Journal of Cancer. 1993;29(7):940–942.

11. Zhang J, FG Stevens M, D Bradshaw T. Temozolomide: mechanisms of action, repair and resistance. Current molecular pharmacology. 2012;5(1):102–114.

12. Mojas N, Lopes M, Jiricny J. Mismatch repair-dependent processing of methylation damage gives rise to persistent single-stranded gaps in newly replicated DNA. Genes & Development. 2007 Dec 15;21(24):3342–55.

13. Roos W, Baumgartner M, Kaina B. Apoptosis triggered by DNA damage O6-methylguanine in human lymphocytes requires DNA replication and is mediated by p53 and Fas/CD95/Apo-1. Oncogene. 2004 Jan;23(2):359–67.

14. Hegi ME, Diserens A-C, Gorlia T, Hamou M-F, de Tribolet N, Weller M, et al. MGMT gene silencing and benefit from temozolomide in glioblastoma. New England Journal of Medicine. 2005;352(10):997–1003.

15. Zhang K, Wang X, Zhou B, Zhang L. The prognostic value of MGMT promoter methylation in Glioblastoma multiforme: a meta-analysis. Familial Cancer. 2013 Sep;12(3):449–58.

16. van den Bent MJ, Carpentier AF, Brandes AA, Sanson M, Taphoorn MJB, Bernsen HJJA, et al. Adjuvant Procarbazine, Lomustine, and Vincristine Improves Progression-Free Survival but Not Overall Survival in Newly Diagnosed Anaplastic Oligodendrogliomas and Oligoastrocytomas: A Randomized European Organisation for Research and Treatment of Cancer Phase III Trial. Journal of Clinical Oncology. 2006 Jun 20;24(18):2715–22.

17. Friedman HS, Prados MD, Wen PY, Mikkelsen T, Schiff D, Abrey LE, et al. Bevacizumab Alone and in Combination With Irinotecan in Recurrent Glioblastoma. Journal of Clinical Oncology. 2009 Oct;27(28):4733–40.

18. Gilbert MR, Dignam JJ, Armstrong TS, Wefel JS, Blumenthal DT, Vogelbaum MA, et al. A Randomized Trial of Bevacizumab for Newly Diagnosed Glioblastoma. New England Journal of Medicine. 2014 Feb 20;370(8):699–708.

19. Ellis HP, Greenslade M, Powell B, Spiteri I, Sottoriva A, Kurian KM. Current Challenges in Glioblastoma: Intratumour Heterogeneity, Residual Disease, and Models to Predict Disease Recurrence. Frontiers in Oncology [Internet]. 2015 Nov 16 [cited 2018 Jan 22];5. Available from: http://journal.frontiersin.org/Article/10.3389/fonc.2015.00251/abstract

20. Ali Arbab, Mohammad Rashid, Kartik Angara, Thaiz Borin, Ping-Chang Lin, Meenu Jain, et al. Major Challenges and Potential Microenvironment-Targeted Therapies in Glioblastoma. International Journal of Molecular Sciences. 2017 Dec 16;18(12):2732.

21. Parker NR, Khong P, Parkinson JF, Howell VM, Wheeler HR. Molecular Heterogeneity in Glioblastoma: Potential Clinical Implications. Frontiers in Oncology [Internet]. 2015 Mar 3 [cited 2018 Jan 22];5. Available from: http://journal.frontiersin.org/Article/10.3389/fonc.2015.00055/abstract

22. Ohgaki H, Kleihues P. The Definition of Primary and Secondary Glioblastoma. Clinical Cancer Research. 2013 Feb 15;19(4):764–72.

23. McLendon R, Friedman A, Bigner D, Van Meir EG, Brat DJ, M. Mastrogianakis G, et al. Comprehensive genomic characterization defines human glioblastoma genes and core pathways. Nature. 2008 Oct 23;455(7216):1061–8.

24. Verhaak RGW, Hoadley KA, Purdom E, Wang V, Qi Y, Wilkerson MD, et al. Integrated Genomic Analysis Identifies Clinically Relevant Subtypes of Glioblastoma Characterized by Abnormalities in PDGFRA, IDH1, EGFR, and NF1. Cancer Cell. 2010 Jan;17(1):98–110.

25. Noushmehr H, Weisenberger DJ, Diefes K, Phillips HS, Pujara K, Berman BP, et al. Identification of a CpG Island Methylator Phenotype that Defines a Distinct Subgroup of Glioma. Cancer Cell. 2010 May;17(5):510–22.

26. Combs SE, Rieken S, Wick W, Abdollahi A, von Deimling A, Debus J, et al. Prognostic significance of IDH-1 and MGMT in patients with glioblastoma: One step forward, and one step back? Radiation Oncology. 2011;6(1):115.

27. Parsons DW, Jones S, Zhang X, Lin JC-H, Leary RJ, Angenendt P, et al. An integrated genomic analysis of human glioblastoma multiforme. Science. 2008;321(5897):1807–1812.

28. IDH1 and IDH2 Mutations in Gliomas. The New England Journal of Medicine. 2009;9.

29. Turcan S, Rohle D, Goenka A, Walsh LA, Fang F, Yilmaz E, et al. IDH1 mutation is sufficient to establish the glioma hypermethylator phenotype. Nature. 2012 Mar;483(7390):479–83.

30. Mao H, LeBrun DG, Yang J, Zhu VF, Li M. Deregulated Signaling Pathways in Glioblastoma Multiforme: Molecular Mechanisms and Therapeutic Targets. Cancer Investigation. 2012 Jan;30(1):48–56.

31. Pearson JRD, Regad T. Targeting cellular pathways in glioblastoma multiforme. Signal Transduction and Targeted Therapy. 2017 Sep 29;2:17040.

32. Brennan CW, Verhaak RGW, McKenna A, Campos B, Noushmehr H, Salama SR, et al. The Somatic Genomic Landscape of Glioblastoma. Cell. 2013 Oct;155(2):462–77.

33. Bastien JIL, McNeill KA, Fine HA. Molecular characterizations of glioblastoma, targeted therapy, and clinical results to date: Molecular Characterizations of Glioblastoma. Cancer. 2015 Feb 15;121(4):502–16.

34. Yang J-M, Schiapparelli P, Nguyen H-N, Igarashi A, Zhang Q, Abbadi S, et al. Characterization of PTEN mutations in brain cancer reveals that pten mono-ubiquitination promotes protein stability and nuclear localization. Oncogene. 2017 Jun;36(26):3673–85.

35. Johnson H, Del Rosario AM, Bryson BD, Schroeder MA, Sarkaria JN, White FM. Molecular Characterization of EGFR and EGFRvIII Signaling Networks in Human Glioblastoma Tumor Xenografts. Molecular & Cellular Proteomics. 2012 Dec;11(12):1724–40.

36. Gont A, Hanson JE, Lavictoire SJ, Parolin DA, Daneshmand M, Restall IJ, et al. PTEN loss represses glioblastoma tumor initiating cell differentiation via inactivation of Lgl1. Oncotarget. 2013;4(8):1266.

37. Gont A, Daneshmand M, Woulfe J, Lavictoire SJ, Lorimer IA. PREX1 integrates G protein-coupled receptor and phosphoinositide 3-kinase signaling to promote glioblastoma invasion. Oncotarget. 2017;8(5):8559.

38. Gont A, Hanson JE, Lavictoire SJ, Daneshmand M, Nicholas G, Woulfe J, et al. Inhibition of glioblastoma malignancy by Lgl1. Oncotarget. 2014;5(22):11541.

39. Lee J, Kotliarova S, Kotliarov Y, Li A, Su Q, Donin NM, et al. Tumor stem cells derived from glioblastomas cultured in bFGF and EGF more closely mirror the phenotype and genotype of primary tumors than do serum-cultured cell lines. Cancer Cell. 2006 May;9(5):391–403.

40. Pollard SM, Yoshikawa K, Clarke ID, Danovi D, Stricker S, Russell R, et al. Glioma Stem Cell Lines Expanded in Adherent Culture Have Tumor-Specific Phenotypes and Are Suitable for Chemical and Genetic Screens. Cell Stem Cell. 2009 Jun;4(6):568–80.

41. Fael Al-Mayhani TM, Ball SLR, Zhao J-W, Fawcett J, Ichimura K, Collins PV, et al. An efficient method for derivation and propagation of glioblastoma cell lines that conserves the molecular profile of their original tumours. Journal of Neuroscience Methods. 2009 Jan;176(2):192–9.

42. Munthe S, Petterson SA, Dahlrot RH, Poulsen FR, Hansen S, Kristensen BW. Glioma Cells in the Tumor Periphery Have a Stem Cell Phenotype. Castro MG, editor. PLOS ONE. 2016 May 12;11(5):e0155106.

43. Li Q, Lin H, Rauch J, Deleyrolle LP, Reynolds BA, Viljoen HJ, et al. Scalable Culturing of Primary Human Glioblastoma Tumor-Initiating Cells with a Cell-Friendly Culture System. Scientific Reports [Internet]. 2018 Dec [cited 2018 May 24];8(1). Available from: http://www.nature.com/articles/s41598-018-21927-4

44. Lathia JD, Mack SC, Mulkearns-Hubert EE, Valentim CLL, Rich JN. Cancer stem cells in glioblastoma. :15.

45. Son MJ, Woolard K, Nam D-H, Lee J, Fine HA. SSEA-1 Is an Enrichment Marker for Tumor-Initiating Cells in Human Glioblastoma. Cell Stem Cell. 2009 May;4(5):440–52.

46. Ogden AT, Waziri AE, Lochhead RA, Fusco D, Lopez K, Ellis JA, et al. IDENTIFICATION OF A2B5+CD133− TUMOR-INITIATING CELLS IN ADULT HUMAN GLIOMAS. Neurosurgery. 2008 Feb 1;62(2):505–15.

47. Rampazzo E, Persano L, Pistollato F, Moro E, Frasson C, Porazzi P, et al. Wnt activation promotes neuronal differentiation of Glioblastoma. Cell Death & Disease. 2013 Feb;4(2):e500–e500.

48. Park NI, Guilhamon P, Desai K, McAdam RF, Langille E, O'Connor M, et al. ASCL1 Reorganizes Chromatin to Direct Neuronal Fate and Suppress Tumorigenicity of Glioblastoma Stem Cells. Cell Stem Cell. 2017 Aug;21(2):209-224.e7.

49. Piccirillo SGM, Reynolds BA, Zanetti N, Lamorte G, Binda E, Broggi G, et al. Bone morphogenetic proteins inhibit the tumorigenic potential of human brain tumour-initiating cells. Nature. 2006 Dec;444(7120):761–5.

50. Carén H, Stricker SH, Bulstrode H, Gagrica S, Johnstone E, Bartlett TE, et al. Glioblastoma Stem Cells Respond to Differentiation Cues but Fail to Undergo Commitment and Terminal Cell-Cycle Arrest. Stem Cell Reports. 2015 Nov;5(5):829–42.

51. Kumar R, Gont A, Perkins TJ, Hanson JEL, Lorimer IAJ. Induction of senescence in primary glioblastoma cells by serum and TGFβ. Scientific Reports [Internet]. 2017 Dec [cited 2018 May 7];7(1). Available from: http://www.nature.com/articles/s41598-017-02380-1

52. Sadahiro H, Yoshikawa K, Ideguchi M, Kajiwara K, Ishii A, Ikeda E, et al. Pathological features of highly invasive glioma stem cells in a mouse xenograft model. Brain Tumor Pathology. 2014 Apr;31(2):77–84.

53. Amin Rustom, Rainer Saffrich, Ivanka Markovic, Paul Walther, Hans-Hermann Gerdes. Nanotubular Highways for Intercellular Organelle Transport. Science. 2004 Feb 13;303(5660):1007–110.

54. Lou E, Gholami S, Romin Y, Thayanithy V, Fujisawa S, Desir S, et al. Imaging Tunneling Membrane Tubes Elucidates Cell Communication in Tumors. Trends in Cancer. 2017 Oct;3(10):678–85.

55. Hanna SJ, McCoy-Simandle K, Miskolci V, Guo P, Cammer M, Hodgson L, et al. The Role of Rho-GTPases and actin polymerization during Macrophage Tunneling Nanotube Biogenesis. Scientific Reports [Internet]. 2017 Dec [cited 2018 Jan 19];7(1). Available from: http://www.nature.com/articles/s41598-017-08950-7

56. Vignais M-L, Caicedo A, Brondello J-M, Jorgensen C. Cell Connections by Tunneling Nanotubes: Effects of Mitochondrial Trafficking on Target Cell Metabolism, Homeostasis, and Response to Therapy. Stem Cells International. 2017;2017:1–14.

57. Delage E, Cervantes DC, Pénard E, Schmitt C, Syan S, Disanza A, et al. Differential identity of Filopodia and Tunneling Nanotubes revealed by the opposite functions of actin regulatory complexes. Scientific Reports [Internet]. 2016 Dec [cited 2018 Jan 19];6(1). Available from: http://www.nature.com/articles/srep39632

58. Gurke S, Barroso JFV, Hodneland E, Bukoreshtliev NV, Schlicker O, Gerdes H-H. Tunneling nanotube (TNT)-like structures facilitate a constitutive, actomyosin-dependent exchange of endocytic organelles between normal rat kidney cells☆. Experimental Cell Research. 2008 Dec 10;314(20):3669–83.

59. Onfelt B, Nedvetzki S, Yanagi K, Davis DM. Cutting Edge: Membrane Nanotubes Connect Immune Cells. The Journal of Immunology. 2004 Aug 1;173(3):1511–3.

60. Thayanithy V, Dickson EL, Steer C, Subramanian S, Lou E. Tumor-stromal cross talk: direct cell-to-cell transfer of oncogenic microRNAs via tunneling nanotubes. Translational Research. 2014 Nov;164(5):359–65.

61. Lou E, Fujisawa S, Morozov A, Barlas A, Romin Y, Dogan Y, et al. Tunneling Nanotubes Provide a Unique Conduit for Intercellular Transfer of Cellular Contents in Human Malignant Pleural Mesothelioma. Yang P-C, editor. PLoS ONE. 2012 Mar 9;7(3):e33093.

62. Burtey A, Wagner M, Hodneland E, Skaftnesmo KO, Schoelermann J, Mondragon IR, et al. Intercellular transfer of transferrin receptor by a contact-, Rab8-dependent mechanism involving tunneling nanotubes. The FASEB Journal. 2015 Nov;29(11):4695–712.

63. Abounit S, Zurzolo C. Wiring through tunneling nanotubes - from electrical signals to organelle transfer. Journal of Cell Science. 2012 Mar 1;125(5):1089–98.

64. Okafo G, Prevedel L, Eugenin E. Tunneling nanotubes (TNT) mediate long-range gap junctional communication: Implications for HIV cell to cell spread. Scientific Reports [Internet]. 2017 Dec [cited 2018 May 13];7(1). Available from: http://www.nature.com/articles/s41598-017-16600-1

65. Gousset K, Schiff E, Langevin C, Marijanovic Z, Caputo A, Browman DT, et al. Prions hijack tunnelling nanotubes for intercellular spread. Nature Cell Biology. 2009 Mar;11(3):328–36.

66. Tardivel M, Bégard S, Bousset L, Dujardin S, Coens A, Melki R, et al. Tunneling nanotube (TNT)-mediated neuron-to neuron transfer of pathological Tau protein assemblies. Acta Neuropathologica Communications [Internet]. 2016 Dec [cited 2018 May 14];4(1). Available from: http://actaneurocomms.biomedcentral.com/articles/10.1186/s40478-016-0386-4

67. Gerdes H-H, Rustom A, Wang X. Tunneling nanotubes, an emerging intercellular communication route in development. Mechanisms of Development. 2013 Jun;130(6–8):381–7.

68. Hase K, Kimura S, Takatsu H, Ohmae M, Kawano S, Kitamura H, et al. M-Sec promotes membrane nanotube formation by interacting with Ral and the exocyst complex. Nature Cell Biology. 2009 Dec;11(12):1427–32.

69. Marzo L, Gousset K, Zurzolo C. Multifaceted Roles of Tunneling Nanotubes in Intercellular Communication. Frontiers in Physiology [Internet]. 2012 [cited 2018 May 14];3. Available from: http://journal.frontiersin.org/article/10.3389/fphys.2012.00072/abstract

70. Sun X, Wang Y, Zhang J, Tu J, Wang X-J, Su X-D, et al. Tunneling-nanotube direction determination in neurons and astrocytes. Cell Death & Disease. 2012 Dec;3(12):e438–e438.

71. Matthias Osswald, Jung E, Sahm F, Solecki G, Venkataramani V, Blaes J. Brain tumour cells interconnect to a functional and resistant network. Nature. 2015;528:93–8.

72. Goslin K, Schreyer D, Pate Skene JH, Banker G. Development of neuronal polarity: GAP-43 distinguishes axonal from dendritic growth cones. Nature. 1988 Dec;336(15):672–4.

73. Haag D, Zipper P, Westrich V, Karra D, Pfleger K, Toedt G, et al. Nos2 Inactivation Promotes the Development of Medulloblastoma in Ptch1+/− Mice by Deregulation of Gap43–Dependent Granule Cell Precursor Migration. Rubin JB, editor. PLoS Genetics. 2012 Mar 15;8(3):e1002572.

74. Osswald M, Solecki G, Wick W, Winkler F. A malignant cellular network in gliomas: potential clinical implications. Neuro-Oncology. 2016 Apr;18(4):479–85.

75. Debanne D. Information processing in the axon. Nature Reviews Neuroscience. 2004 Apr;5(4):304–16.

76. Lewis TL, Courchet J, Polleux F. Cellular and molecular mechanisms underlying axon formation, growth, and branching. The Journal of Cell Biology. 2013 Sep 16;202(6):837–48.

77. Kevenaar JT, Hoogenraad CC. The axonal cytoskeleton: from organization to function. Frontiers in Molecular Neuroscience [Internet]. 2015 Aug 14 [cited 2018 May 17];8. Available from: http://journal.frontiersin.org/Article/10.3389/fnmol.2015.00044/abstract

78. Wang D, Bordey A. The astrocyte odyssey. Progress in Neurobiology [Internet]. 2008 Oct 1 [cited 2018 May 18]; Available from: http://linkinghub.elsevier.com/retrieve/pii/S030100820800110X

79. Rodnight RB, Gottfried C. Morphological plasticity of rodent astroglia. Journal of Neurochemistry. 2013 Feb;124(3):263–75.

80. Kimelberg HK, Nedergaard M. Functions of astrocytes and their potential as therapeutic targets. Neurotherapeutics. 2010 Oct;7(4):338–53.

81. Ramirez-Weber F-A, Kornberg TB. Cytonemes: Cellular Processes that Project to the Principal Signaling Center in Drosophila Imaginal Discs. Cell. 97:599–607.

82. Kornberg TB, Roy S. Cytonemes as specialized signaling filopodia. Development. 2014 Feb 15;141(4):729–36.

83. Snyder JC, Rochelle LK, Marion S, Lyerly HK, Barak LS, Caron MG. Lgr4 and Lgr5 drive the formation of long actin-rich cytoneme-like membrane protrusions. Journal of Cell Science. 2015 Mar 15;128(6):1230–40.

84. Sebé-Pedrós A, Burkhardt P, Sánchez-Pons N, Fairclough SR, Lang BF, King N, et al. Insights into the Origin of Metazoan Filopodia and Microvilli. Molecular Biology and Evolution. 2013 Sep;30(9):2013–23.

85. Mattila PK, Lappalainen P. Filopodia: molecular architecture and cellular functions. Nature Reviews Molecular Cell Biology. 2008 Jun;9(6):446–54.

86. Chang K, Baginski J, Hassan SF, Volin M, Shukla D, Tiwari V. Filopodia and Viruses: An Analysis of Membrane Processes in Entry Mechanisms. Frontiers in Microbiology [Internet]. 2016 Mar 10 [cited 2018 May 20];7. Available from: http://journal.frontiersin.org/Article/10.3389/fmicb.2016.00300/abstract

87. Yamaguchi H, Condeelis J. Regulation of the actin cytoskeleton in cancer cell migration and invasion. Biochimica et Biophysica Acta (BBA) - Molecular Cell Research. 2007 May;1773(5):642–52.

88. Lucato CM, Halls ML, Ooms LM, Liu H-J, Mitchell CA, Whisstock JC, et al. The Phosphatidylinositol (3,4,5)-Trisphosphate-dependent Rac Exchanger 1·Ras-related C3 Botulinum Toxin Substrate 1 (P-Rex1·Rac1) Complex Reveals the Basis of Rac1 Activation in Breast Cancer Cells. Journal of Biological Chemistry. 2015 Aug 21;290(34):20827–40.

89. Vara JÁF, Casado E, de Castro J, Cejas P, Belda-Iniesta C, González-Barón M. PI3K/Akt signalling pathway and cancer. Cancer Treatment Reviews. 2004 Apr;30(2):193–204.

90. Welch HC. Regulation and function of P-Rex family Rac-GEFs. Small GTPases. 2015 Apr 3;6(2):49–70.

91. Bid HK, Roberts RD, Manchanda PK, Houghton PJ. RAC1: An Emerging Therapeutic Option for Targeting Cancer Angiogenesis and Metastasis. Molecular Cancer Therapeutics. 2013 Oct 1;12(10):1925–34.

92. Bos JL, Rehmann H, Wittinghofer A. GEFs and GAPs: Critical Elements in the Control of Small G Proteins. Cell. 2007 Jun;129(5):865–77.

93. Raftopoulou M, Hall A. Cell migration: Rho GTPases lead the way. Developmental Biology. 2004 Jan;265(1):23–32.

94. Hanna S, El-Sibai M. Signaling networks of Rho GTPases in cell motility. Cellular Signalling. 2013 Oct;25(10):1955–61.

95. Stankiewicz TR, Linseman DA. Rho family GTPases: key players in neuronal development, neuronal survival, and neurodegeneration. Frontiers in Cellular Neuroscience [Internet]. 2014 Oct 7 [cited 2018 Jan 19];8. Available from: http://journal.frontiersin.org/article/10.3389/fncel.2014.00314/abstract

96. Lawson CD, Ridley AJ. Rho GTPase signaling complexes in cell migration and invasion. The Journal of Cell Biology. 2018 Feb 5;217(2):447–57.

97. Welch HCE, Coadwell WJ, Ellson CD, Ferguson GJ, Andrews SR, Erdjument-Bromage H, et al. P-Rex1, a PtdIns(3,4,5)P3- and G□-Regulated Guanine-Nucleotide Exchange Factor for Rac. :13.

98. Welch HCE, Condliffe AM, Milne LJ, Ferguson GJ, Hill K, Webb LMC, et al. P-Rex1 Regulates Neutrophil Function. Current Biology. 2005 Oct;15(20):1867–73.

99. Mayeenuddin LH, Garrison JC. Phosphorylation of P-Rex1 by the Cyclic AMP-dependent Protein Kinase Inhibits the Phosphatidylinositiol (3,4,5)-Trisphosphate and Gβγ-mediated Regulation of Its Activity. Journal of Biological Chemistry. 2006 Jan 27;281(4):1921–8.

100. Marei H, Carpy A, Woroniuk A, Vennin C, White G, Timpson P, et al. Differential Rac1 signalling by guanine nucleotide exchange factors implicates FLII in regulating Rac1-driven cell migration. Nature Communications. 2016 Feb 18;7:10664.

101. Moriyama K. Two activities of cofilin, severing and accelerating directional depolymerization of actin filaments, are affected differentially by mutations around the actin-binding helix. The EMBO Journal. 1999 Dec 1;18(23):6752–61.

102. Edwards DC, Sanders LC, Bokoch GM, Gill GN. Activation of LIM-kinase by Pak1 couples Rac/Cdc42 GTPase signalling to actin cytoskeletal dynamics. Nature Cell Biology. 1999 Sep;1(5):253–9.

103. Arber S, Barbayannis FA, Hanser H, Schneider C, Stanyon CA, Bernard O, et al. Regulation of actin dynamics through phosphorylation of cofilin by LIM-kinase. Nature. 1998 Jun;393(6687):805–9.

104. Marei H, Malliri A. GEFs: Dual regulation of Rac1 signaling. Small GTPases. 2017 Apr 3;8(2):90–9.

105. Tomasevic N, Jia Z, Russell A, Fujii T, Hartman JJ, Clancy S, et al. Differential Regulation of WASP and N-WASP by Cdc42, Rac1, Nck, and PI(4,5)P2. Biochemistry. 2007 Mar;46(11):3494–502.

106. Sanz-Moreno V. Tumour Invasion: A New Twist on Rac-Driven Mesenchymal Migration. Current Biology. 2012 Jun;22(11):R449–51.

107. Kato T, Kawai K, Egami Y, Kakehi Y, Araki N. Rac1-Dependent Lamellipodial Motility in Prostate Cancer PC-3 Cells Revealed by Optogenetic Control of Rac1 Activity. Nie D, editor. PLoS ONE. 2014 May 21;9(5):e97749.

108. Chen B, Gao Y, Jiang T, Ding J, Zeng Y, Xu R, et al. Inhibition of Tumor Cell Migration and Invasion Through Knockdown of Rac1 Expression in Medulloblastoma Cells. Cellular and Molecular Neurobiology. 2011 Mar;31(2):251–7.

109. Lindsay CR, Lawn S, Campbell AD, Faller WJ, Rambow F, Mort RL, et al. P-Rex1 is required for efficient melanoblast migration and melanoma metastasis. Nature Communications. 2011 Nov 22;2:555.

110. Montero JC, Seoane S, Ocaña A, Pandiella A. P-Rex1 participates in Neuregulin-ErbB signal transduction and its expression correlates with patient outcome in breast cancer. Oncogene. 2011 Mar;30(9):1059–71.

111. Sosa MS, Lopez-Haber C, Yang C, Wang H, Lemmon MA, Busillo JM, et al. Identification of the Rac-GEF P-Rex1 as an Essential Mediator of ErbB Signaling in Breast Cancer. Molecular Cell. 2010 Dec;40(6):877–92.

112. Mense SM, Barrows D, Hodakoski C, Steinbach N, Schoenfeld D, Su W, et al. PTEN inhibits PREX2-catalyzed activation of RAC1 to restrain tumor cell invasion. Science Signaling. 2015 Mar 31;8(370):ra32–ra32.

113. Lissanu Deribe Y, Shi Y, Rai K, Nezi L, Amin SB, Wu C-C, et al. Truncating PREX2 mutations activate its GEF activity and alter gene expression regulation in NRAS-mutant melanoma. Proceedings of the National Academy of Sciences. 2016 Mar 1;113(9):E1296–305.

114. Lathia JD, Gallagher J, Heddleston JM, Wang J, Eyler CE, MacSwords J, et al. Integrin Alpha 6 Regulates Glioblastoma Stem Cells. Cell Stem Cell. 2010 May;6(5):421–32.

115. Lathia JD, Li M, Hall PE, Gallagher J, Hale JS, Wu Q, et al. Laminin alpha 2 enables glioblastoma stem cell growth. Annals of Neurology. 2012 Nov;72(5):766–78.

116. Kaufman LJ, Brangwynne CP, Kasza KE, Filippidi E, Gordon VD, Deisboeck TS, et al. Glioma Expansion in Collagen I Matrices: Analyzing Collagen Concentration-Dependent Growth and Motility Patterns. Biophysical Journal. 2005 Jul;89(1):635–50.

117. Florczyk SJ, Wang K, Jana S, Wood DL, Sytsma SK, Sham JG, et al. Porous chitosan-hyaluronic acid scaffolds as a mimic of glioblastoma microenvironment ECM. Biomaterials. 2013 Dec;34(38):10143–50.

118. Gordon V. Measuring the mechanical stress induced by an expanding multicellular tumor system: a case study. Experimental Cell Research. 2003 Sep 10;289(1):58–66.

119. Ran FA, Hsu PD, Wright J, Agarwala V, Scott DA, Zhang F. Genome engineering using the CRISPR-Cas9 system. Nature Protocols. 2013 Oct 24;8(11):2281–308.

120. Jinek M, Chylinski K, Fonfara I, Hauer M, Doudna JA, Charpentier E. A Programmable Dual-RNA-Guided DNA Endonuclease in Adaptive Bacterial Immunity. Science. 2012 Aug 17;337(6096):816–21.

121. Su T, Liu F, Gu P, Jin H, Chang Y, Wang Q, et al. A CRISPR-Cas9 Assisted Non-Homologous End-Joining Strategy for One-step Engineering of Bacterial Genome. Scientific Reports [Internet]. 2016 Dec [cited 2018 May 21];6(1). Available from: http://www.nature.com/articles/srep37895

122. Guan C, Kumar S, Kucera R, Ewel A. Changing the Enzymatic Activity of T7 Endonuclease by Mutations at the β-Bridge Site: Alteration of Substrate Specificity Profile and Metal Ion Requirements by Mutation Distant from the Catalytic Domain. Biochemistry. 2004 Apr;43(14):4313–22.

123. Babon JJ, McKenzie M, Cotton RGH. The use of resolvases T4 endonuclease VII and T7 endonuclease I in mutation detection. MOLECULAR BIOTECHNOLOGY. 2003;23:9.

124. Ostrom QT, Bauchet L, Davis FG, Deltour I, Fisher JL, Langer CE, et al. The epidemiology of glioma in adults: a "state of the science" review. Neuro-Oncology. 2014 Jul 1;16(7):896–913.

125. Jung E, Osswald M, Blaes J, Wiestler B, Sahm F, Schmenger T, et al. Tweety-Homolog 1 Drives Brain Colonization of Gliomas. The Journal of Neuroscience. 2017 Jul 19;37(29):6837–50.

126. Chauveau A, Aucher A, Eissmann P, Vivier E, Davis DM. Membrane nanotubes facilitate long-distance interactions between natural killer cells and target cells. Proceedings of the National Academy of Sciences. 2010 Mar 23;107(12):5545–50.

127. Sowinski S, Jolly C, Berninghausen O, Purbhoo MA, Chauveau A, Köhler K, et al. Membrane nanotubes physically connect T cells over long distances presenting a novel route for HIV-1 transmission. Nature cell biology. 2008;10(2):211–219.

128. Hamzei-Sichani F, Kamasawa N, Janssen WGM, Yasumura T, Davidson KGV, Hof PR, et al. Gap junctions on hippocampal mossy fiber axons demonstrated by thin-section electron microscopy and freeze fracture replica immunogold labeling. Proceedings of the National Academy of Sciences. 2007 Jul 24;104(30):12548–53.

129. Elias LAB, Turmaine M, Parnavelas JG, Kriegstein AR. Connexin 43 Mediates the Tangential to Radial Migratory Switch in Ventrally Derived Cortical Interneurons. Journal of Neuroscience. 2010 May 19;30(20):7072–7.

130. Sosinsky GE, Nicholson BJ. Structural organization of gap junction channels. Biochimica et Biophysica Acta (BBA) - Biomembranes. 2005 Jun;1711(2):99–125.

131. Chen R, Nishimura MC, Bumbaca SM, Kharbanda S, Forrest WF, Kasman IM, et al. A Hierarchy of Self-Renewing Tumor-Initiating Cell Types in Glioblastoma. Cancer Cell. 2010 Apr;17(4):362–75.

132. Gielen PR, Aftab Q, Ma N, Chen VC, Hong X, Lozinsky S, et al. Connexin43 confers Temozolomide resistance in human glioma cells by modulating the mitochondrial apoptosis pathway. Neuropharmacology. 2013 Dec;75:539–48.

133. Thuringer D, Berthenet K, Cronier L, Solary E, Garrido C. Primary tumor- and metastasis-derived colon cancer cells differently modulate connexin expression and function in human capillary endothelial cells. Oncotarget [Internet]. 2015 Oct 6 [cited 2018 May 8];6(30). Available from: http://www.oncotarget.com/fulltext/4894

134. Burkovetskaya M, Karpuk N, Xiong J, Bosch M, Boska MD, Takeuchi H, et al. Evidence for Aberrant Astrocyte Hemichannel Activity in Juvenile Neuronal Ceroid Lipofuscinosis (JNCL). Kira J, editor. PLoS ONE. 2014 Apr 15;9(4):e95023.

135. Kinjo ER, Higa GSV, Morya E, Valle AC, Kihara AH, Britto LRG. Reciprocal Regulation of Epileptiform Neuronal Oscillations and Electrical Synapses in the Rat Hippocampus. Charpier S, editor. PLoS ONE. 2014 Oct 9;9(10):e109149.

136. Pereira MSL, Zenki K, Cavalheiro MM, Thomé CC, Filippi-Chiela EC, Lenz G, et al. Cellular Senescence Induced by Prolonged Subculture Adversely Affects Glutamate Uptake in C6 Lineage. Neurochemical Research. 2014 May;39(5):973–84.

137. Lee K, Kentroti S, Billie H, Bruce C, Vernadakis A. Comparative biochemical, morphological, and immunocytochemical studies between C-6 glial cells of early and late passages and advanced passages of glial cells derived from aged mouse cerebral hemispheres. Glia. 1992;6(4):245–57.

138. Chen W, Wang D, Du X, He Y, Chen S, Shao Q, et al. Glioma cells escaped from cytotoxicity of temozolomide and vincristine by communicating with human astrocytes. Medical Oncology [Internet]. 2015 Mar [cited 2018 May 8];32(3). Available from: http://link.springer.com/10.1007/s12032-015-0487-0

139. Yusubalieva GM, Baklaushev VP, Gurina OI, Zorkina YA, Gubskii IL, Kobyakov GL, et al. Treatment of Poorly Differentiated Glioma Using a Combination of Monoclonal Antibodies to Extracellular Connexin-43 Fragment, Temozolomide, and Radiotherapy. Bulletin of Experimental Biology and Medicine. 2014 Aug;157(4):510–5.

140. Munoz JL, Rodriguez-Cruz V, Greco SJ, Ramkissoon SH, Ligon KL, Rameshwar P. Temozolomide resistance in glioblastoma cells occurs partly through epidermal growth factor receptor-mediated induction of connexin 43. Cell Death & Disease. 2017 Mar;5(3):e1145–e1145.

141. Murphy SF, Varghese RT, Lamouille S, Guo S, Pridham KJ, Kanabur P, et al. Connexin 43 Inhibition Sensitizes Chemoresistant Glioblastoma Cells to Temozolomide. Cancer Research. 2016 Jan 1;76(1):139–49.

142. Cairncross G, Wang M, Shaw E, Jenkins R, Brachman D, Buckner J, et al. Phase III Trial of Chemoradiotherapy for Anaplastic Oligodendroglioma: Long-Term Results of RTOG 9402. Journal of Clinical Oncology. 2013 Jan 20;31(3):337–43.

143. Wharton SB, Maltby E, Jellinek DA, Levy D, Atkey N, Hibberd S, et al. Subtypes of oligodendroglioma defined by 1p,19q deletions, differ in the proportion of apoptotic cells but not in replication-licensed non-proliferating cells. Acta Neuropathologica. 2007 Jan 23;113(2):119–27.